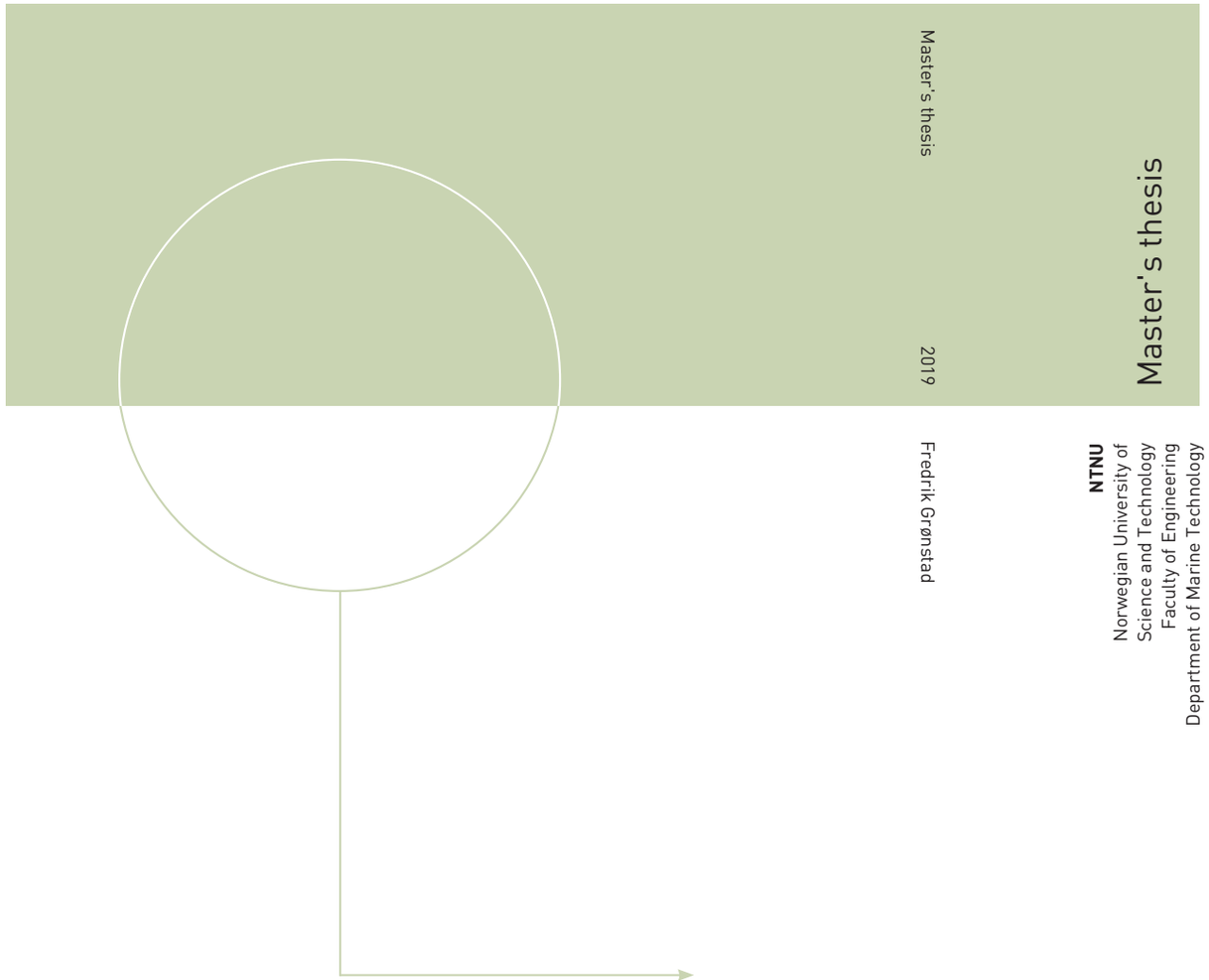

Master's thesis

2019

Fredrik Grønstad

NTNU
Norwegian University of
Science and Technology
Faculty of Engineering
Department of Marine Technology

Fredrik Grønstad

Modelling and Simulation of Underwater Vehicle-Manipulator System

July 2019

NTNU
Norwegian University of
Science and Technology

NTNU
Norwegian University of
Science and Technology

NTNU

Norwegian University of
Science and Technology

Modelling and Simulation of Underwater Vehicle-Manipulator System

Fredrik Grønstad

Marine Cybernetics
Submission date: July 2019
Supervisor: Martin Ludvigsen

Norwegian University of Science and Technology
Department of Marine Technology

Preface

This master thesis is based on the research carried out during the spring semester of 2019 at the Department of Marine Technology, Norwegian University of Science and Technology. The main topics of this thesis mathematical modelling of underwater vehicle-manipulator system, and a robotic manipulator affects the response and movement of a remotely operated vehicle submerged in water. This work is a result of individual work and study, and help from my supervisor, Martin Ludvigsen. This master thesis has been a challenging task, but it has been rewarding and taught me a lot. I want to express my gratitude to Martin Ludvigsen and Stein Melvær Nornes, for valuable comments and remarks regarding the draft of this thesis.

Trondheim, July 2019

Fredrik Grønstad

Abstract

This master thesis considers the interaction between a manipulator and a Remotely Operated Vehicle (ROV), as a Underwater Vehicle-Manipulator System (UVMS). The Norwegian University of Science and Technology have developed a new ROV, Minerva 2, which is considered in this thesis. There are mainly two aspects which is focused upon in this project, the mathematical modelling of the UVMS, and how the manipulator with different configurations and joint rotations, is affecting the ROV.

The mathematical modelling of the UVMS is done by considering a second order differential equation, often called mass-damper-spring system, to derive the equation of motion for the system. Mass properties is used to determine the rigid body motion, while hydrodynamic parameters and matrices have been established in order to account for the effect of being submerged in water. The matrices describing the dynamics of the manipulator are dependent on the configuration of the manipulator, and is therefore needed to be calculated every iteration of the simulation.

Kinematic modelling of the manipulator was developed according the Denavit-Hartenberg (DH) convention. The relation between each link is found by assigning a reference frame in each module, and by knowing the distance between each joint, a rotation transformation is performed in order to translate from one reference frame to another. The kinematics are used to determine the position and orientation of the end-effector, given the different joint angles.

Simulink is the platform used to perform the simulations. The equation of motion of the UVMS is modelled as a block diagram in the Laplace domain. Several simulations were conducted, the manipulator configurations were varying and movements to the joints were added, to observe how the manipulator affected the response of the ROV.

Sammendrag

Denne masteroppgaven omhandler samspillet mellom en manipulator og en fjernstyrt undervannskjøretøy, dette systemet blir også kalt et undervanns kjøretøy-manipulator system. Norges Tekniske og Naturvitenskapelige Univeristet har utviklet en ny fjernstyrt undervannskjøretøy, Minerva 2, som er i fokus i denne masteroppgaven. Det er i hovedsak to aspekter som er fokusert på i dette prosjektet, og det er den matematiske modelleringen av undervanns kjøretøy-manipulator systemet, og hvordan manipulatoren ved forskjellige konfigurasjoner og bevegelser, påvirker Minerva 2.

Den matematiske modelleringen av systemet er gjort ved å vurdere en andre ordens differensialligning, ofte kalt masse-fjær-demper-system, for å utlede bevegelsesligningen for systemet. Massegenskapene brukes til å bestemme bevegelsen til det stive legemet, mens de hydrodynamiske parameterne og matrisene er etablert for å ta i betraktning effekten av å være nedsenket i vann. Matrisene som beskriver manipulatorens dynamikk er avhengig av manipulatorens konfigurasjon, og er derfor beregnet i hver iterasjon av simuleringene.

Den kinematiske modelleringen av manipulatoren ble utviklet i henhold til Denavit-Hartenberg (DH) konvensjonen. Forholdet mellom hver manipulator del ble funnet ved å tilordne et referansesystem i hvert ledd, og ved å i tillegg vite avstanden mellom hvert ledd, blir en rotasjonstransformasjon brukt til å transformere egenskaper fra et referansesystem til et annet. Kinematikken brukes til å bestemme posisjonen og orienteringen til endeeffektoren, gitt de forskjellige leddvinklene.

Simulink er plattformen som brukes til å utføre simuleringene. Bevegelsesligningen til undervanns kjøretøy-manipulator systemet er modellert som et blokkskjema i Laplace-domenet. Flere simuleringer ble utført, hvor manipulatorkonfigurasjonene varierte og rotasjoner i leddene ble påsatt for å observere hvordan manipulatoren påvirket responsen til Minerva 2.

Contents

List of Figures **VII**

List of Tables **IX**

Abbreviations **XI**

1 Introduction **1**
1.1 Background and Motivation 1
1.1.1 Remotely Operated Vehicles 3
1.1.2 Manipulators 5
1.1.3 Underwater Vehicle-Manipulator Systems 8
1.2 Minerva 2 8
1.3 Litterature Study 11
1.4 Project Structure 13

2 Rigid Body Kinematics **15**
2.1 Rigid Body Kinematics 15
2.1.1 Reference Frames 15
2.1.2 Euler Angles 16
2.1.3 The Rotation Matrix 16
2.2 Quaternion Orientation Representation 18
2.3 Rigid Body Transformations 19

3 Rigid Body Dynamics **23**
3.1 Rigid Body Dynamics 23
3.1.1 Assumptions 23
3.1.2 Governing Equations 23

4 Manipulator Kinematics **31**
4.1 Kinematics 32
4.1.1 Denavit Hartenberg Convention 32
4.1.2 Direct Kinematics 34

4.1.3 Inverse Kinematics . . . 36
4.2 Twists . . . 39
4.3 Static Forces and Moments in the Manipulator . . . 40
4.3.1 Jacobian Matrix . . . 41
4.3.2 Joint Torques . . . 42
4.3.3 Force Propagation . . . 42

5 Manipulator Dynamics **45**
5.1 Kinetic and Potential Energy in Multibody Systems . . . 45
5.2 Equation of Motion . . . 46

6 Dynamics of Underwater Vehicle-Manipulator System **49**
6.1 Dynamics . . . 49

7 Method **55**
7.1 UVMS Model . . . 55
7.1.1 Dynamic Matrices . . . 56
7.1.2 Measure States . . . 56
7.2 Numerical Values of the Matrices Used in the Simulations . . . 59

8 Results **61**
8.1 Manipulator in Stowed Position . . . 61
8.2 Manipulator Fully Extended . . . 62
8.2.1 Standing Still . . . 63
8.2.2 Moving . . . 63
8.3 Manipulator Oriented Downwards . . . 64
8.3.1 Standing Still . . . 64
8.3.2 Moving . . . 65

9 Discussion **67**
9.1 Manipulator in Stowed Position . . . 67
9.2 Manipulator Fully Extended . . . 68
9.3 Manipulator Oriented Downwards . . . 69

10 Conclusion **71**
10.1 Further Work . . . 71

Appendices **73**

A Differentiation of Jacobian Matrix **75**

B Derivation of $\mathbf{W}_i$ **77**

List of Figures

1.1 Typical AUV and ROV designs 1
1.2 Different ROV classes 4
1.3 Orion 7R Manipulator 5
1.4 Dimension of Orion 7R 7
1.5 CAD model of Minerva 2 9

2.1 Coordinate frames attached to the Vehicle-Manipulator System 16
2.2 The orientation of a rigid body represented by reference frame $\mathscr{F}_b$ with basis $\{e_x^{'}, e_y^{'}, e_z^{'}\}$ with respect to an inertial reference frame $\mathscr{F}_0$ with basis $\{e_x, e_y, e_z\}$ for rotations with one and three degrees of freedom 17

4.1 Manipulator system, Orion 7R 31
4.2 Coordinate frames satisfying the DH assumptions 33
4.3 Schematic representation of the coordinate-axes used to determine DH parameters and homogeneous transformation matrices 34
4.4 Three link manipulator 37
4.5 Three link manipulator with two solutions 37

7.1 Underwater vehicle-manipulator system modelled in *Simulink* 55
7.2 Calculation of dynamic matrices 56
7.3 Calculation of dynamic matrices 57
7.4 Calculation of dynamic matrices 58
7.5 Calculation of dynamic matrices 58

8.1 Response of the system to a stowed manipulator 62
8.2 Response when the manipulator is at its full reach 63
8.3 Response when the manipulator is fully extended and moving 64
8.4 Response when the manipulator is standing still and oriented downwards 65
8.5 Response when the manipulator is configured downwards 66

List of Tables

1.1 Specification of Orion 7R 6
1.2 Rotation capability of each joint 7
1.3 Angles of the thrusters 11
1.4 Positions of the thruster relative to COG in body frame 11

4.1 Denavit-Hartenberg Parameters 34
4.2 Calculate the Jacobian 41

Abbreviations

AUV Autonomous Underwater Vehicle

COB Center of Buoyancy

COG Center of Gravity

DH Denavit-Hartenberg

DOF Degree of Freedom

DP Dynamic Positioning

DVL Doppler Velocity Log

EOM Equation of Motion

IMU Inertial Measurement Unit

ROV Remotely Operated Vehicle

UUV Unmanned Underwater Vehicle

UVMS Underwater Vehicle-Manipulator Systems

Chapter 1

Introduction

1.1 Background and Motivation

The ocean plays a significant part to the habitants of the earth. It covers about 71 % of the earth's surface, and it provides us with resources, energy, transportation and numerous other beneficial possibilities. Yet, only 5 % of the ocean space is discovered. It was not possible to reach great depth until recent years, because of the lack of appropriate technology. But with the introduction of the Unmanned Underwater Vehicles (UUV) in the 20'th century, the deepest parts, for the first time in history, are now accessible to the mankind. New technology, reduced costs and improved sensors have made it possible to produce underwater vehicle systems for both commercial and recreational use. The application range of the UUVs is very broad, for instance they are commonly used in the oil and gas industry, for structural inspection and installation, science and research, such as seabed mapping, marine biology and oceanographic research. Based on this, it is fair to say that the ocean currently is and always will be, in the foreseeable future, an important development platform.

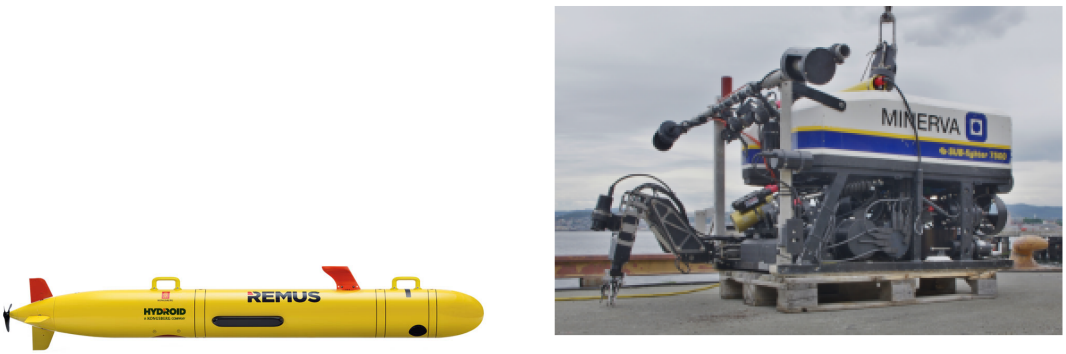

(a) AUV Remus100 **(b)** ROV Minerva

Figure 1.1: Typical AUV and ROV designs

There are mainly two types of UUVs, Remotely Operated Vehicles (ROV) and Autonomous Underwater Vehicles (AUV). Physically, these are mainly distinguished by whether or not they are tethered. ROVs requires educated personnel to control the vehicle. Since the staff is located above the sea surface, the control of the ROV is dependent on a tether to transfer the signals from the operation room to the ROV. This causes restrictions of the survey area, since the tether has limits considering the length. ROV are mostly used for inspection, maintenance and repair, due their high payload and maneuvering capabilities. AUVs on the other hand, is not dependent on any tether to operate, and can therefore cover larger areas. Additionally, with their high speed and autonomous capabilities, it makes them suited for monitoring and mapping of the seabed, which is where they are most commonly used. Since the AUVs are not dependent on any tethers, the power source needs to be mounted on board. Thus, the power consumption is of great concern. In order to minimize the power consumption, the AUV need to be hydrodynamic and as light as possible. Hence, the most common shape of AUV is today torpedo-like. This shape brings small hydrodynamic forces, which makes it possible to achieve high speed with respect to minimal power consumption. These types of AUVs are controlled by vertical and horizontal control fins, which makes the maneuverability properties of the vehicles quite limited, and therefore not well designed for intervention tasks.

ROVs on the other hand has very limited autonomy properties, where the more advanced autonomy functionality that is installed on working class ROV today is dynamic positioning (DP) or station keeping systems. Autonomous functionalities often requires navigation and guidance, which also includes localization and and path planning (Eidsvik 2018). These tasks are done by the operator through an umbilical cable. However, the development of the ROV tends towards increasing the level of autonomy, to make it able to perform intervention and inspection tasks on its own. Since ROV are equipped with thrusters in multiple degrees of freedom (DOF), it is able to maintain good maneuverability at low speed, and therefore it is capable to perform intervention tasks. However, the complex shape of the ROV and the difficulty of predicting the response that comes with it, makes it hard to design controllers. Hence, the use of the human operator.

Since the industry always looks for more cost efficient methods, the development of the ROV tends, as stated earlier, towards autonomy. Here, the human operator is not needed anymore, and a great expense is eliminated. By introducing autonomous ROVs, the time efficiency will also increase, because being dependent on an operator, takes up a lot of time. Considerable amount of training and education isd required in order to be approved to control the ROV, as well as the person has to be present under the whole task duration. Therefore, implementing autonomous systems results in higher efficiency and reduced costs.

The development of autonomous system in ROV has made progress and results. In the early stages of the ROV history, the operator had to control each thurster individually. However, automatic depth control simplified the operation, as the ROV commonly are neutrally buoyant. The development of control systems that automated the process

of maintaining positions and tracking, enabled the pilot to focus on monitoring and planning of operations that requires human intervention and decision making (Dukan 2014). Hence, developing methods, models and tools to estimate the response of the ROVs is important in order to design better control schemes that can contribute to more autonomous systems, as well as aiding the human operators.

1.1.1 Remotely Operated Vehicles

ROVs are usually dived into classes depending on their purpose. According to (Standard-Norge 2003), ROVs are mainly divided into five different classes:

Class I - Pure Observation: Pure observation ROVs are physically limited to video observation. They are mainly equipped with a video camera, lights and thrusters. Without considerable amount of modifications, they can only perform observation operations.

Class II - Observation with payload option: Observation ROV that have the capability of carrying at least two additional sensors, are classified as a Class II ROV. The added sensors are often still colour video cameras, cathodic protection measurement systems, additional video cameras and sonar systems. It is required that the Class II ROV maintain the capability of operating without loss of original function while carrying additional payload, such as other sensors.

Class III - Work class vehicles: Class III vehicles are vehicles that are large enough to carry additional sensors and/or manipulators. These vehicles often have multiplexing capability which allows the additional sensors and tools to operate without being hardwired thorugh the umbilical cables. Clas III is then again sub-divided into three groups dependent on their horse power (Hp).

- Class III A - Workclass vehicles < 100 Hp
- Class III B - Workclass vehicles 100 Hp to 150 Hp
- Class III C - Workclass vehicles > 150 Hp

Class IV - Seabed-working vehicles: Seabed-working vehicles maneuver on the seabed by using wheels or belt traction system, thrusters or water jets, or by combinations of these. These types of vehicles are often much larger and heavier than a Class III ROV, and this is because they are often used in cable and pipeline trenching, excavation, dredging and other seabed operations, that requires a lot of force.

Class V - Prototype or development vehicles: Class V includes the vehicles that are being developed or those regarded prototypes. Special-purpose ROVs, such as seabed-working vehicles, can also be assigned as Class V vehicles. Currently, AUVs are also assigned to Class V.

(a) Class I ROV, BlueROV 2

(b) Class II ROV, H1000

(c) Class III ROV, Minerva

(d) Class IV ROV, vLBC

Figure 1.2: Different ROV classes

Today, the workclass ROV is the most common ROV type that used in installation-, maintenance- and repair operations in the industry. This is because of the high payload capacity and the ability to operate in deep water. According to estimates from (Group 2018), the world's ROV expenditure will total more than $ 10 billion between 2018-2022. The majority of these operations will be performed by workclass ROVs. ROVs usually consists of a set of thrusters, that makes it possible to control the ROV in all the desired DOFs, sensors, for instance inertial measurement units (IMU), magnetometers or gyro compasses, acoustic transceivers, and Doppler velocity logs (DVL), as well as mission related tools, such as manipulators, lights and video cameras. Workclass ROVs are usually designed with a large metacentric height to

maintain proper stability with respect to rotation around its horizontal axes (roll and pitch). In addition to a large metacentric height, ROV are often equipped with movable ballast and buoyancy elements, with the purpose to shift the center of gravity (COG) and/or center of buoyancy (COB) to accommodate for varying operational conditions.

1.1.2 Manipulators

Workclass ROVs are often equipped with one or two manipulators, depending on the type of operation the ROV is designed for. The main reason for equipping ROVs with manipulators is to design it for intervention tasks. With mounting the ROV with manipulators, additional hydrodynamic, hydrostatic and rigid body inertia forces and moments will affect the vehicle (Schjølberg 1996). If the ROV is large enough, these effects are negligible. However, these effects usually have to be modelled and taken into account when designing workclass ROVs. Here the manipulator is of considerable size, and the presence of the manipulator will create forces and moments on the ROV that affects the response of the system. In addition, when the manipulators performs intervention tasks, they come in contact with the environment, which creates contact forces that also will affect the ROV. No matter the size difference between the ROV and the manipulator, the contact forces can be of considerable size, that needs to be taken into account when modelling the system.

The manipulator used in this thesis, Orion 7R, is shown in Figure 4.1. This is a 7 DOF manipulator produced by FMC Technologies Schilling Robotics. It is a compact and light-weight manipulator system designed for light- and medium-class ROVs. The arm's structural segments are fabricated from hard-anodized extruded aluminum for strength and corrosion resistance (Robotics 2013).

Figure 1.3: Orion 7R Manipulator

Orion 7R is equipped with position sensors which are magnetically coupled and sealed in titanium housings, and all of the servo valves and subsea-electronics are in one

enclosure. The specifications of the Orion 7R is presented in Table **??**.

Table 1.1: Specification of Orion 7R

Parameter	Value
Reach	1532 [mm]
Materials	Anodized Aluminium, Stainless steel, Titanium
DOFs	7
Standard Depth	6500 [msw]
Weight in air	54 [kg]
Weight in water	38 [kg]
Lift at full extension	68 [kg]
Maximum lift, nominal	250 [kg]
Standard Gripper Opening	97 [mm]
Grip Force, nominal	4448 [N]
Wrist Torque, nominal	205 [Nm]
Wrist Rotate, continuous	6-35 [rpm]

The dimension of each module of the manipulator is seen in Figure 1.4a - 1.4c. These Figures gives an overview of all the dimensions of Orion 7R, as well as a planar and elevation view when fully extended.

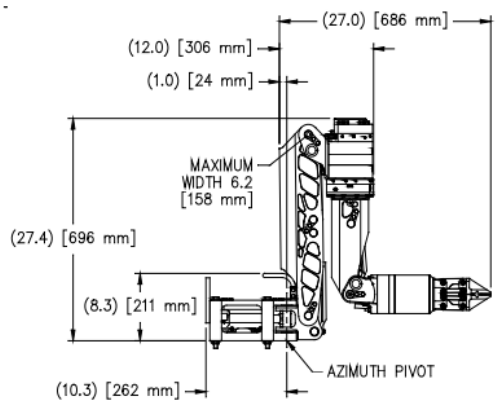

(a) Stow Dimensions

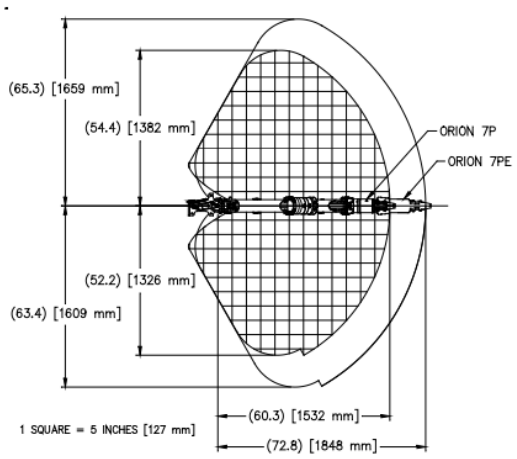

(b) Planar View

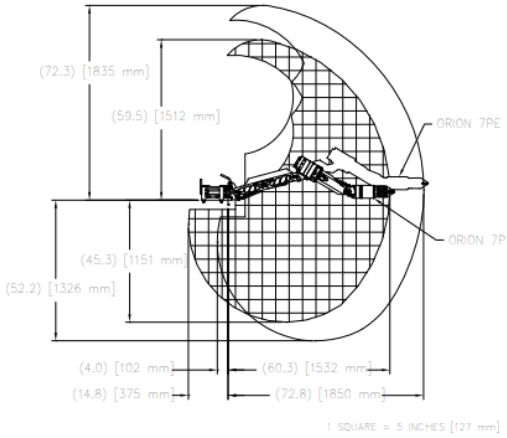

(c) Elevation View

Figure 1.4: Dimension of Orion 7R

Each of the joints is capable of rotating in at least one direction, and these rotations can be seen in Table 1.2.

Table 1.2: Rotation capability of each joint

Joint	Degree of Rotation
Base Yaw, Linear	120°
Shoulder Pitch, Linear	120°
Elbow Pitch, Linear	120°
Forearm Roll, Rotary	270°
Wrist Pitch, Linear	120°
Wrist Roll, Rotary	360°

1.1.3 Underwater Vehicle-Manipulator Systems

A Underwater Vehicle-Manipulator System (UVMS) is an underwater robot intended to operate with dexterity in workspace larger than for a manipulator with a fixed base. Manipulators are designed to handle and manipulate objects with dexterity and accuracy, but the fixed base limits the workspace. Therefore, mounting the manipulator on a underwater vehicle, the workspace would significantly improve. A UVMS consists therefore of

- A base, normally with actuation, which can move freely in a given environment.
- One or more manipulator arms mounted on the base.

As stated, it is the base that provides the mobility of the system, and enables it to move across large geographical areas. For UVMS, the geographical area is restricted to under water, and some of the important working areas are:

- The vehicle is docked an an ocean pipeline while the manipulator perform maintenance work.
- The manipulator performs service tasks while the vehicle is at a fixed position.
- The vehicle follows an ocean pipeline while the manipulator performs inspection around the pipe.

There are many different task and services the UVMS can provide. The underwater environment is not very accessible to humans. Therefore, as UVMS can operate in deep waters and over large geographical area, it has received increased amount of attention in later years. This means, underwater robots can be utilized where humans either cannot or do not want to operate as the health risks are too great.

1.2 Minerva 2

The ROV considered in this master thesis is the Minerva 2. This is the new ROV developed by NTNU, and is shown in Figure 1.5.

Figure 1.5: CAD model of Minerva 2

This is a working class ROV with a mass of 1500 $[kg]$, and it is equipped with forward look multibeam sonar, acoustic underwater positioning and navigation systems, such as HiPAP, and DVLs and IMUs for position measurements. The ROV has seven thrusters available, where four of them are placed in the horizontal plane. The remaining three thruster are position in a vertical plane (Holven 2018). To avoid water being flushed through the vehicle, the thrusters are slightly tilted, and all of them are have an fixed orientation. The geometry is presented in Figure 1.6a, 1.6b and 1.6c. These figures shows the thruster geometry in the xz-plane, xy-plane and yz-plane, respectively. The coordinate system is oriented so the x-axis is directed to port, y-axis is directed upwards and the z-axis is directed forward. The different positions and angles presented in these figures are shown in Table 1.3 and 1.4.

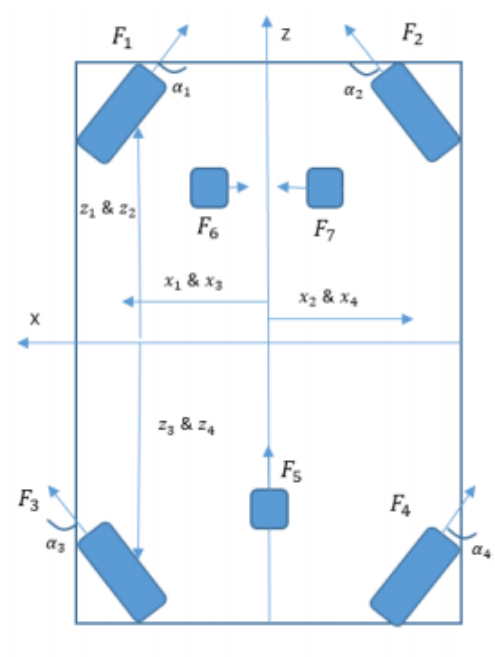

(a) Sketch of the thruster setup for Minerva 2 in the x-z plane

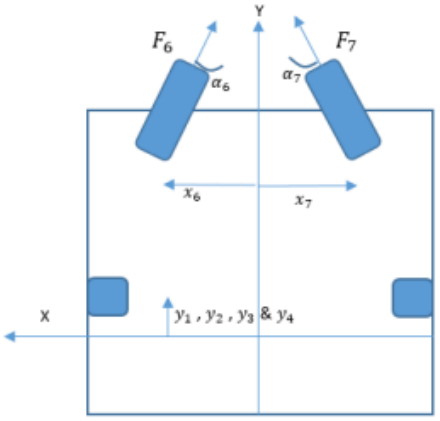

(b) Sketch of the thruster setup for Minerva 2 in the x-y plane

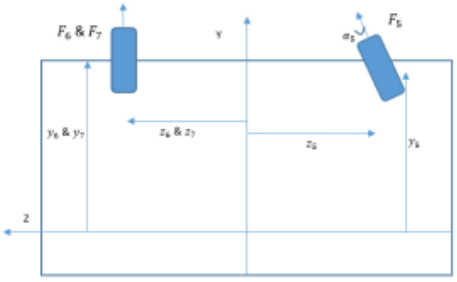

(c) Sketch of the thruster setup for Minerva 2 in the y-z plane

Table 1.3: Angles of the thrusters

Thruster nr.	Symbol	Angle [Deg]
1	α_1	45
2	α_2	-45
3	α_3	-45
4	α_4	45
5	α_5	15
6	α_6	-30
7	α_7	30

Table 1.4: Positions of the thruster relative to COG in body frame

Thruster nr.	X [mm]	Y [mm]	Z [mm]
1	520	165	920
2	-520	165	920
3	520	165	-920
4	-520	165	-920
5	0	231.37	-940.19
6	575.71	284.68	550
7	-575.71	284.68	550

1.3 Litterature Study

Current research and development of underwater vehicles is extensively tending towards making ROVs more autonomous. Since these are the vehicles mainly used in underwater operations, these types of vehicles are in focus. To be able to perform intervention tasks, they need to be equipped with some sort of manipulators, and in order to perform, the dynamics of this coupled system need to be modelled appropriately. If the modelling is not sufficient enough, making controllers or autonomous system suitable to control the system, would be difficult. Therefore, in recent years, different methods to model the dynamics have been proposed in various literature.

In 1995 (Mcmillan, Orin, and Mcghee 1995) presented an algorithm that had been developed for a dynamic simulation of an underwater vehicle equipped with a manipulator. The basis for this method was a land-based algorithm, since these already had

several efficient algorithm to date. This system is using articulated bodies, and is more computationally efficient compared to Newton-Euler approaches, which is usually used in in ROV-manipulator modelling. Hydrodynamic effect on rigid bodies, such as added mass, drag, fluid acceleration and buoyancy forces are incorporated in the system. Furthermore, this result is extended to systems with serial chains of rigid bodies, and efficiently added into the algorithm. One main advantage of this method and framework is its ability to simulate and make computations on a variety of models in which the hydrodynamic forces on a link is a function of velocity and acceleration.

The same year, 1995, (Mclain, Rock, and M. Lee 1995) presented another approach on how to perform the coordinated control of the ROV and manipulator system, where they also tested this method experimentally. It was shown that the dynamic interaction between the robotic arm and the underwater vehicle was very significant as it moves through water. By using a new highly accurate approach to model the hydrodynamic interaction forces, which was developed as a part of this study, a coordinated arm/vehicle control strategy was implemented. The dynamic interaction forces acting on the vehicle due to the manipulator arm was predicted and fed forward into the control system. This resulted in a greatly enhanced station-keeping capability, and the tracking errors and settling times for the manipulator's end point was significantly reduced. Hence, correctly modelling of the manipulator and ROV interaction can significantly increase the performance of the ROV system.

(Schjølberg 1996) presented a model of the combined ROV and manipulator dynamics on matrix-vector form by utilizing the Newton-Euler approach. The recursive Newton-Euler approach is extended to include added mass forces, vortex-induced forces, buoyant forces, rotational damping moments and current loads acting on an underwater manipulator. The dynamics of the manipulator is written on matrix form, and the equation of motion of the vehicle is retrieved taking into account forces from the manipulator acting on the vehicle. The model has the benefit of simplifying nonlinear control theory, whereas, for instance, the feedback linearization technique is evaluated through simulation of decoupling schemes. The total equation of motion is written in a matrix-form where structural properties like symmetry, skew-symmetry and positiveness are established. This simplifies the control design and enables the use of Lyapunov stability theory, which is beneficial.

Jee-Hwan Ryu and Dong-Soo Kwon from *Korea Advanced Institute of Science and Technology* (Ryu, Kwon, and P.-M. Lee 2001) presented in 2001 a scheme for obtaining high maneuverability of underwater robot manipulators mounted on a ROV. To compensate for the dynamic interaction between the manipulator and ROV, force-torque (F/T) information between the manipulator and the vehicle is used to regulate the states of the ROV. When the F/T sensor was not available,aobserver was used to take its place. This paper proposes a disturbance observer to estimate the forces between the manipulator and vehicle. To obtain the dynamics of the system, Euler-Lagrange method was applied, and this formulation was used to test how a feed-forward based observer could counteract the buoyancy and inertia forces arising from the interaction with the robotic arm. The obtained results from this paper showed that the observer

were able to counteract these forces, and therefore were able to significantly improve the trajectory tracking and the performance of the ROV.

(Sarkar and Podder 2001) came up with a new motion coordination algorithm in 2001 for autonomous underwater manipulator-vehicle system. The dynamics behind this system is derived from using Quasi-Lagrange formulation. The algorithm generates desired trajectories for both the vehicle and the manipulator with respect to minimize the total hydrodynamic drag on the system. The Quasi-Lagrange formulation brings the benefit of representing the kinetic and potential energy in the body-fixed frame of the vehicle rather than the inertial frame. The fact the velocity is represented in the body-fixed frame, also simplifies the implementation of the feed-forward control. The results of the work show promise and indicates potential of the proposed approach regarding to provide a useful motion planning framework for underwater robotic systems. However, all the results are from computer simulations, hence, all the uncertainties and complexities of a real world environment might not have been captured. Therefore, further testing of this approach is required in order to to verify the suitability and the advantages for an autonomous system.

Just last year, (Huang et al. 2017) published an article about general modeling of an unmanned underwater vehicle and manipulator using an Newton-Euler approach. The equation of motion of the total system is given by:

$$\mathbf{M_{RB}}(\mathbf{q})\dot{\nu} + \mathbf{C_{RB}}(\mathbf{q},\nu)\nu + \mathbf{M_A}(\mathbf{q})\dot{\nu_r} + \mathbf{C_A}(\mathbf{q},\nu_\mathbf{r})\nu_\mathbf{r} + \mathbf{D}(\mathbf{q},\nu_\mathbf{r})\nu_\mathbf{r} + \mathbf{g}(\mathbf{q}) + \tau_{\mathbf{Mmom}} = \tau_{\mathbf{ctrl}}, \tag{1.1}$$

where ν is the velocity vector of the vehicle, $\mathbf{q}$ is the generalized coordinate vector of the manipulator joints, $\mathbf{M_{RB}}$ is mass matrix, $\mathbf{C_{RB}}$ is the Coriolis and centripetal matrix, $\nu_\mathbf{r}$ is the relative velocity vector relative to the ocean current, $\mathbf{M_A}(\mathbf{q})$ is the added mass matrix, $\mathbf{C_A}(\mathbf{q},)$ is the Coriolis and centripetal added mass matrix, $\mathbf{D}(\mathbf{q},\nu_\mathbf{r})$ is the hydrodynamic drag matrix, $\mathbf{g}(\mathbf{q})$ is the restoring forces and moments vector, $\tau_{\mathbf{ctrl}}$ is the control forces and moments vector and $\tau_{\mathbf{Mmom}}$ represents the coupling forces and moments between the vehicle and manipulator during manipulation. Recursive Newton-Euler formulation was used to calculate the joint forces, and the coupling forces and moments was determined by evaluating the first joint, joint 1. A 3-link manipulator was investigated, and the presented model was synthesized into a numerical simulator, and the response from the forces and moments was inspected. The simulations from this method showed that manipulator movements created large enough moments to make the vehicle roll and pitch violently. Hence, the forces from the manipulator need to be counteracted by a controller to avoid critical rotations.

1.4 Project Structure

Chapter 2-6 of this thesis will cover the relevant theory. Here the mathematical modelling of the ROV, the manipulator and the combined underwater vehicle-manipulator

system is presented. Chapter 7 concerns the method used to simulate the system, and how results are retrieved. Chapter 8 is the result section. Here the simulations are presented and the result of the ROV's displacement and rotations when exposed to different manipulator configurations and movements. Afterwards the results are analyzed and discussed in Chapter 9, before Chapter 10 concludes the thesis and proposes possibilities and relevant further work areas.

Chapter 2

Rigid Body Kinematics

2.1 Rigid Body Kinematics

Kinematics treats the geometrical aspect of motion, and any dynamics analysis starts off with a kinematic study. It defines the admissible configurations and velocities without taking what causes the motion into account. The location of a rigid body is described by its position and orientation. The position is given by the location of the origin of the reference frame attached to the body with respect to an inertial reference frame, and the orientation is described by representing the coordinate axis, of the reference frame attached to the rigid body, in the inertial reference frame (Fossen 2011).

2.1.1 Reference Frames

The reference frames used to represent the position and orientation of the vehicle system in $\mathbb{R}^3$ is shown in Figure 2.1. The system consists of six independent coordinates, three for position and three Euler angles for the orientation. A body-fixed reference frame, denoted *Frame B*, is fixed in the vehicle body, and an inertial frame, denoted *Frame I*, is similar reference frame fixed in space. The body-fixed reference frame is a moving coordinate frame, and its position and orientation is described relative to the inertial reference frame. To describe the configuration and kinematics of the manipulator, a frame is attached to each link according to the Denavit-Hartenberg convention, where the number of reference frames, are determined by the number of links N. The base frame is denoted *Frame 0*, while the reference frame attached to link N is denoted *Frame N*.

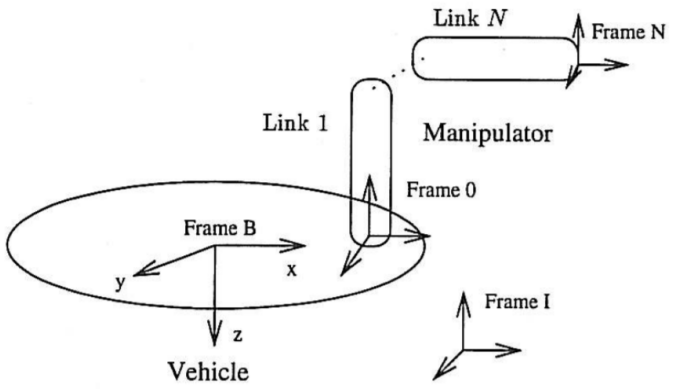

Figure 2.1: Coordinate frames attached to the Vehicle-Manipulator System

2.1.2 Euler Angles

A commonly used representation of the vehicle orientation is the Euler angles representation. The orientation of a rigid body is given by a sequence of three rotations about the coordinate axes. There are many different sequences, 12 in total, and the most common ones are ZYX, ZXZ and ZYZ, which are often referred to as Euler angles type I, II and III, respectively. The ZYX Euler angles are known as the roll, pitch and yaw angles, and are often used to describe the orientation of marine vessels and vehicles.

2.1.3 The Rotation Matrix

Any orientation can be achieved by composing three elemental rotation, where the starting configuration is known. Equivalently, any rotation matrix can be decomposed into a product of the rotation matrices. If we write the basis of a rigid body as $\{e_x^{'}, e_y^{'}, e_z^{'}\}$, this can be written in term of the inertial coordinate frame $\{e_x, e_y, e_z\}$ as

$$e_x^{'} = r_{xx}e_x + r_{xy}e_y + r_{xz}e_z \tag{2.1}$$
$$e_y^{'} = r_{yx}e_x + r_{yy}e_y + r_{yz}e_z \tag{2.2}$$
$$e_z^{'} = r_{zx}e_x + r_{zy}e_y + r_{zz}e_z \tag{2.3}$$

Alternatively, this can be written as

$$\begin{bmatrix} e_x^{'} \\ e_y^{'} \\ e_z^{'} \end{bmatrix} = \begin{bmatrix} r_1 & r_2 & r_3 \end{bmatrix} \begin{bmatrix} e_x \\ e_y \\ e_z \end{bmatrix} \tag{2.4}$$

where the vectors r_1, r_2 and r_3 are coordinates of the base $\{e_x^{'}, e_y^{'} e_z^{'}\}$ relative to $\{e_x, e_y, e_z\}$. The matrix

$$\mathbf{R} = \begin{bmatrix} r_1 & r_2 & r_3 \end{bmatrix} \tag{2.5}$$

is called the *Rotation matrix*. There are numerous ways to determine the rotation matrix, but by following one of the sequences mentioned in the previous section, the ZYX Euler angles, we first rotate an angle ϕ about the x-axis, represented by $\mathbf{R}_x(\phi)$, then a rotation θ about the y-axis, represented by $\mathbf{R}_y(\theta)$, and lastly a rotation ψ about the z-axis, represented as $\mathbf{R}_z(\psi)$. A single rotation about the x-axis can be seen in Figure 2.2a, and a three consecutive rotation can be seen in Figure 2.2b.

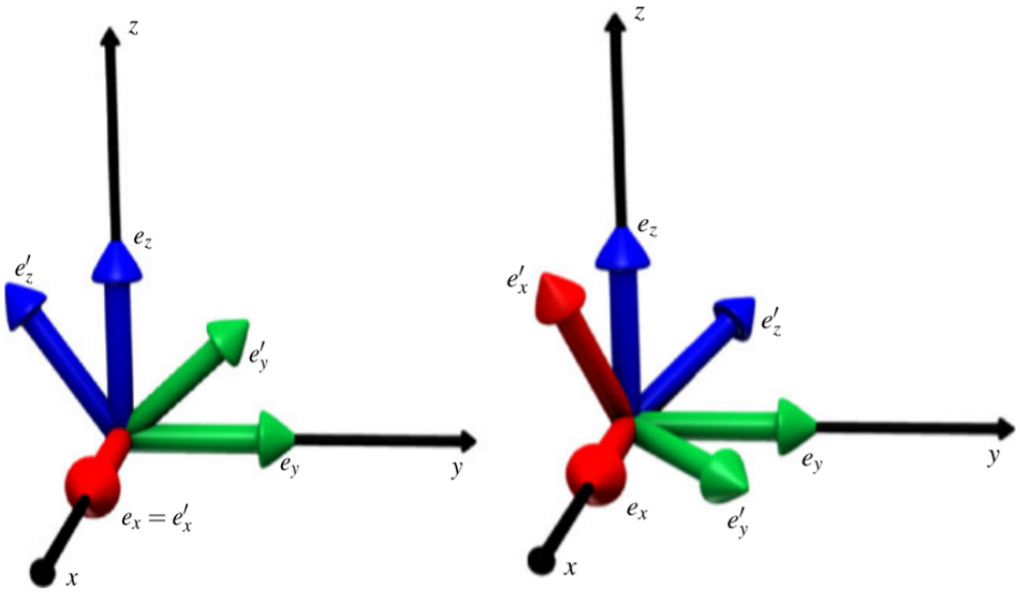

(a) Rotation about the x-axis **(b)** A three consecutive rotation

Figure 2.2: The orientation of a rigid body represented by reference frame $\mathscr{F}_b$ with basis $\{e_x^{'}, e_y^{'}, e_z^{'}\}$ with respect to an inertial reference frame $\mathscr{F}_0$ with basis $\{e_x, e_y, e_z\}$ for rotations with one and three degrees of freedom

Hence, the rotation matrix can be written as

$$\mathbf{R} = \mathbf{R}_z(\psi)\mathbf{R}_y(\theta)\mathbf{R}_x(\phi) \quad \in \mathbb{R}^{3\times 3} \tag{2.6}$$

The rotation matrix gives a complete description of the orientation of a rigid body with reference frame $\mathscr{F}_b$ relative to an inertial frame $\mathscr{F}_0$. The rotation matrix can also be used to rotate a vector $p^{\hat{\imath}}$, observed in reference frame i, into the same vector p^j, observed in reference frame, j, by

$$\mathbf{p}^i = \mathbf{R}_{ji}\mathbf{p}^j \tag{2.7}$$

where $\mathbf{R}_{ji}$ is the rotation matrix from reference frame i to reference frame j. The column vector of the rotation matrix represents the unit vectors of a orthonormal frame i.e.

$$r_i^T r_j = \begin{cases} 0, & \text{for i} \neq \text{j}, \\ 1, & \text{for i} = \text{j}. \end{cases}$$

The orthogonality and unity conditions adds three restrictions to the rotation matrix. Since the rotation matrix consists of nine elements, we see that the orientation of the rigid body has three degrees of freedom. The conditions can also be written as

$$\mathbf{R}\mathbf{R}^T = \mathbf{R}^T\mathbf{R} = \mathbf{I} \tag{2.8}$$

and by post multiplying with R^{-1} we get

$$\mathbf{R}^T = \mathbf{R}^{-1} \tag{2.9}$$

which is a property frequently used, and often simplifies problems.

2.2 Quaternion Orientation Representation

An alternative to the Euler angles representation, is the use of quaternions. This is a four-parameter method based on unit quaternions. The main motivation to use four parameters to represent an orientation is to avoid the Euler angle singularities. A quaternion is a complex number consisting of one real part, $\boldsymbol{\eta}$, and the imaginary parts given by

$$\boldsymbol{\epsilon} = [\epsilon_1\ \epsilon_2\ \epsilon_3]^T \tag{2.10}$$

The set Q of quaternions, satisfying $\mathbf{q^T q} = 1$, is defined as

$$\mathbf{Q} = \left\{\mathbf{q} | \mathbf{q^T q} = 1, \mathbf{q} = [\eta\ \boldsymbol{\epsilon}^T]^T\ \boldsymbol{\epsilon} \in \mathbb{R}^3 \text{and}\ \boldsymbol{\eta} \in \mathbb{R}\right\} \tag{2.11}$$

The scalar part η and the vector part ϵ of the quaternion represent a rotation by an angle β around an unit axis λ, and are defined as:

$$\eta := \cos\frac{\beta}{2} \tag{2.12}$$

$$\epsilon = [\epsilon_1\ \epsilon_2\ \epsilon_3] := \boldsymbol{\lambda}\sin\frac{\beta}{2} \tag{2.13}$$

where $\boldsymbol{\lambda} = [\lambda_1\ \lambda_2\ \lambda_3]^T$ is a unit vector satisfying

$$\boldsymbol{\lambda} = \pm\frac{\boldsymbol{\epsilon}}{\sqrt{\boldsymbol{\epsilon}^T\boldsymbol{\epsilon}}} \text{if} \sqrt{\boldsymbol{\epsilon}^{\boldsymbol{T}}\boldsymbol{\epsilon}} \neq 0 \tag{2.14}$$

Hence, the following parametrization is valid

$$\mathbf{q} = \begin{bmatrix} \eta \\ \epsilon_1 \\ \epsilon_2 \\ \epsilon_3 \end{bmatrix} = \begin{bmatrix} \cos\frac{\beta}{2} \\ \boldsymbol{\lambda}\sin\frac{\beta}{2} \end{bmatrix} \in \mathbf{Q} \qquad 0 \leq \beta \leq 2\pi \tag{2.15}$$

This also implies that the unit quaternion satisfy the constraint $\mathbf{q^T q} = 1$, that is

$$\eta^2 + \epsilon_1^2 + \epsilon_2^2 + \epsilon_3^2 = 1 \tag{2.16}$$

The coordinate transformation matrix for the unit quaternion, can be expressed as (Fossen 2011):

$$\mathbf{R_b^n}(\mathbf{q}) := \mathbf{R}_{\eta,\boldsymbol{\epsilon}} = \mathbf{I}_{3\times 3} + 2\eta\mathbf{S}(\boldsymbol{\epsilon}) + 2\mathbf{S^2}(\boldsymbol{\epsilon}) \tag{2.17}$$

2.3 Rigid Body Transformations

A rigid body's location is described by the position and orientation of a reference frame attached to the body with respect to the inertial frame. The configuration of the body frame is found by firstly represent the origin of the body frame with respect to the inertial frame, as seen from the inertial frame, and secondly write the orientation of the body frame with respect to the inertial frame as if they were coinciding.

Commonly, the position and velocity vector of the rigid body is presented as

$$\boldsymbol{\eta} = \begin{bmatrix} x \\ y \\ z \\ \phi \\ \theta \\ \psi \end{bmatrix}, \quad \boldsymbol{\nu} = \begin{bmatrix} u \\ v \\ w \\ p \\ q \\ r \end{bmatrix} \tag{2.18}$$

The position vector, $\boldsymbol{\eta}$, is defined in the global reference frame, NED, and the velocity vector, $\boldsymbol{\nu}$, is described in the body fixed reference frame.

In order to establish a model representing, and since the position vector, $\boldsymbol{\eta}$, and the velocity vector, $\boldsymbol{\nu}$, is defined in different reference frames, a mapping between them is established. The relation between the derivative of the position vector, $\dot{\boldsymbol{\nu}}$, and the body velocity vector, $\boldsymbol{\nu}$, is given by

$$\dot{\boldsymbol{\eta}} = \boldsymbol{J}(\boldsymbol{\eta})\boldsymbol{\nu} \tag{2.19}$$

where $\mathbf{J}$ is the rotation transformation matrix defined as

$$\mathbf{J} = \begin{bmatrix} \mathbf{R}_{\mathbf{b}}^{\mathbf{n}}(\boldsymbol{\Theta}) & \mathbf{0}_{3\times 3} \\ \mathbf{0}_{3\times 3} & \mathbf{T}_{\boldsymbol{\Theta}}(\boldsymbol{\Theta}) \end{bmatrix} \tag{2.20}$$

$\mathbf{R}_{\mathbf{b}}^{\mathbf{n}}$ is the rotation matrix from the body frame to NED frame, $\boldsymbol{\Theta}$ denotes the Euler angles $[\phi\ \theta\ \psi]$ and $\mathbf{T}_{\boldsymbol{\Theta}}$ is a transformation matrix relating the body fixed angular velocities $\boldsymbol{\omega} = [p, q, r]$ and the Euler angles $\boldsymbol{\Theta}$. By utilizing the ZYX rotation sequence, the transformation matrix can be written as

$$\mathbf{T}_{\boldsymbol{\Theta}}(\boldsymbol{\Theta}) = \begin{bmatrix} 1 & \sin\phi\cos\theta & \cos\phi\tan\theta \\ 0 & \cos\phi & -\sin\phi \\ 0 & \frac{\sin\phi}{\cos\theta} & \frac{\cos\phi}{\cos\theta} \end{bmatrix} \tag{2.21}$$

Hence the velocity transformation matrix is given by

$$\begin{bmatrix} x \\ y \\ z \\ \phi \\ \theta \\ \psi \end{bmatrix} = \begin{bmatrix} c\psi c\theta & c\psi s\theta s\psi - s\psi c\phi & c\psi c\phi s\theta + s\psi s\phi & 0 & 0 & 0 \\ s\psi c\theta & s\phi s\theta s\psi + c\phi c\phi & s\theta s c\phi - c\psi s\phi & 0 & 0 & 0 \\ -s\theta & c\theta s\phi & c\theta c\phi & 0 & 0 & 0 \\ 0 & 0 & 0 & 1 & \frac{s\phi s\theta}{c\theta} & \frac{c\phi s\theta}{c\theta} \\ 0 & 0 & 0 & 0 & c\phi & -s\phi \\ 0 & 0 & 0 & 0 & \frac{s\phi}{c\theta} & \frac{c\phi}{c\theta} \end{bmatrix} \begin{bmatrix} u \\ v \\ w \\ p \\ q \\ r \end{bmatrix} \tag{2.22}$$

where $s(\cdot)$ and $c(\cdot)$ denotes sin and cos, respectively. It can be observed from Equation (2.22) that $\mathbf{T}_{\boldsymbol{\Theta}}$, and thus $\mathbf{J}$, is not defined for $\theta = \pm\frac{\pi}{2}$. This is the Euler angle singularity, and it appears for the ZYX-sequence as θ reaches $\pm\frac{\pi}{2}$. The singularity is results of the operation where the terms are divided by $c\theta$, since $\cos\pm\frac{\pi}{2} = 0$.

The velocity transformation describes the kinematics of a rigid body motion in $\mathbb{R}^6$ when the velocities are represented in the body frame. On the other hand, if the velocities is preferred represented in the inertial frame, the reverse relation is given by a velocity transformation matrix given as

$$\mathbf{J} = \begin{bmatrix} \mathbf{I} & \mathbf{0_{3\times 3}} \\ \mathbf{0_{3\times 3}} & \mathbf{T_{\Theta}}(\mathbf{R_b^n})^{-1} \end{bmatrix} \tag{2.23}$$

Chapter 3

Rigid Body Dynamics

3.1 Rigid Body Dynamics

This section considers the dynamics of the ROV. The relevant models and tools used to determine the dynamic properties of the system is presented, and how the different parameters are determined.

3.1.1 Assumptions

When modelling a physical system, assumptions are made to either simplify the system of even making it possible to model it. A common assumption to make in hydrodynamic modelling is to say that the fluid is viscid and incompressible.

An uncoupled system is another assumption often made, the off-diagonal parameters of the mass matrix and damper matrix are very difficult to identify. From (Fossen 2011), this assumption is made by saying that ROV are only allowed to operate at low speeds. If the velocities are too large, the motion will be highly nonlinear and coupled, and the assumption in invalid. If the ROV has three planes of symmetry, which can be assumed in the ROV case, one can justify that the contributions of the off-diagonal parameters of the added mass matrix and damping matrix can be neglected compared to the diagonal elements (Fossen 2011).

3.1.2 Governing Equations

In order to represent a physical problem accurately, a set of governing equations needs to be established. Since the system is a non-flexible underwater vehicle, the equation of motion can be deduced from Newton's 2nd law. The forces and moment acting on the body, is described by:

$$\boldsymbol{\tau}_{RB} = \tau_{hyd} + \boldsymbol{\tau}_{hs} + \boldsymbol{\tau}_{cable} + \boldsymbol{\tau}_{manipulator} + \boldsymbol{\tau} \tag{3.1}$$

where τ_{RB} are the inertia forces and moments acting on the body, τ_{hyd} are the hydrodynamic forces and moments, τ_{hs} are hydrostatic restoring forces, τ_{cable} are cable forces and moments, $\tau_{manipulator}$ are the manipulator forces and moments and τ are the thruster forces and moments.

For marine crafts it is desireable to derive the Equation of Motion (EOM) for an arbitrary origin, CO, to take advantage of the craft's geometric properties. Since the hydrodynamic forces and moments are computed in CO, the EOM is also expressed from CO. The rigid body dynamics in a body-fixed reference frame located at CO are obtained from the Newton-Euler equations of motion (Fossen 2011). The obtained expression is as following,

$$\boldsymbol{\tau}_{RB} = \begin{bmatrix} \mathbf{F}_{RB} \\ \mathbf{m}_{RB} \end{bmatrix} = \begin{bmatrix} m[\dot{\boldsymbol{\nu}} + \dot{\boldsymbol{\omega}} \times \mathbf{r} + \boldsymbol{\omega} \times \boldsymbol{\nu} + \boldsymbol{\omega} \times (\boldsymbol{\omega} \times \mathbf{r})] \\ \mathbf{I}\dot{\boldsymbol{\omega}} + \boldsymbol{\omega} \times \mathbf{I}\boldsymbol{\omega} + m\mathbf{r} \times (\dot{\boldsymbol{\nu}} + \boldsymbol{\omega} \times \boldsymbol{\nu}) \end{bmatrix} \tag{3.2}$$

where $\mathbf{F}_{RB}$ are the inertial forces, $\mathbf{m}_{RB}$ are the inertial moments, ν are the linear velocities, ω are the angular velocities and $\mathbf{r}$ is the vector from the body-fixed reference frame to the centre of gravity of the ROV. The inertial forces and moments are expressed in the body-fixed reference frame, while the linear and angular velocities are expressed in the body-fixed reference frame origin relative to the inertial reference frame origin. According to (Fossen 2011), Equation 3.2 can also be written in a vectorial setting:

$$\tau_{RB} = \mathbf{M}_{RB}\dot{\nu} + \mathbf{C}_{RB}(\nu)\nu, \tag{3.3}$$

where $\mathbf{M}_{RB}$ is the rigid body mass matrix, $\mathbf{C}_{RB}$ represents the Coriolis and centripetal vector term from Equation 3.2 and ν is generalized velocity vector. If the Coriolis and centripetal matrix $\mathbf{C}_{RB}$ is parametrized independent of linear velocity, $\nu = [u, v, w]^T$, and the ocean current is irrotational and constant, the rigid body kinetics satisfies (Fossen 2011)

$$\boldsymbol{\tau}_{RB} = \mathbf{M}_{RB}\dot{\boldsymbol{\nu}}_r + \mathbf{C}_{RB}(\boldsymbol{\nu}_r)\boldsymbol{\nu}_r, \tag{3.4}$$

where ν_r is the relative velocity due to the current,

$$\boldsymbol{\nu}_r = \begin{bmatrix} \boldsymbol{\nu} - \boldsymbol{\nu}_c \\ \boldsymbol{\omega} \end{bmatrix} \tag{3.5}$$

and $\mathbf{M_{RB}}$ is given by:

$$\mathbf{M_{RB}} = \begin{bmatrix} m\mathbf{I_{3\times 3}} & -m\mathbf{S}(\mathbf{r_g^b}) \\ m\mathbf{S}(\mathbf{r_g^b}) & \mathbf{I_g} - m\mathbf{S}^2(\mathbf{r_g^b}) \end{bmatrix} \tag{3.6}$$

$$= \begin{bmatrix} m & 0 & 0 & 0 & mz_g & -my_g \\ 0 & m & 0 & -mz_g & 0 & mx_g \\ 0 & 0 & m & my_g & -mx_g & 0 \\ 0 & -mz_g & -my_g & I_x & -I_{xy} & -I_{zx} \\ mz_g & 0 & -mx_g & -I_{xy} & I_y & -I_{yz} \\ -my_g & mx_g & 0 & -I_{zx} & -I_{yz} & I_z \end{bmatrix} \tag{3.7}$$

Where m is the mass of the body, $\mathbf{r_g^b} = [x_g, y_g, z_g]$ is the vector form the origin to the center of gravity (COG), $\mathbf{I_g}$ is the inertia matrix and the I_{ij} term denotes the moments of inertia about the origin. The other matrix term, $\mathbf{C_{RB}}$ in Equation 3.4 is given by:

$$\mathbf{C_{RB}}(\nu) = \begin{bmatrix} m\mathbf{S}(\nu_2) & -m\mathbf{S}(\nu_2)\mathbf{S}(\mathbf{r}_g^b) \\ m\mathbf{S}(\mathbf{r}_g^b)\mathbf{S}(\boldsymbol{\nu}_2) & -\mathbf{S}(\mathbf{I}_b\nu_2) \end{bmatrix} \tag{3.8}$$

For a body that is submerged in any fluid, a buoyancy force will appear. This is a result of the displaced fluid, and will act as a force in the center of buoyancy (COB), which is the centre of mass of the displaced fluid. Since the centre of gravity and center of buoyancy does not always coincide, these two forces will act on different locations on the body, which makes moments arise. A submerged body is stable if the COB is located above the COG. This is because any perturbations from this state will create a lever arm between the forces and therefore generate moments counteracting the displacement. The net force and moments in the 6 DOF is derived as shown in Equation 3.9.

$$\boldsymbol{\tau}_{hs} = \mathbf{g}(\eta) = \begin{bmatrix} (W-B)\sin\theta \\ -(W-B)\cos\theta\sin\phi \\ -(W-B)\cos\theta\cos\phi \\ -(y_gW - y_bB)\cos\theta\cos\phi + (z_gW - z_bB)\cos\theta\sin\phi \\ (z_gW - z_bB)\sin\theta + (x_gW - x_bB)\cos\theta\cos\phi \\ -(x_gW - x_bB)\cos\theta\sin\phi - (y_gW - y_bB)\sin\theta \end{bmatrix} \tag{3.9}$$

W is the weight of the vehicle, B is buoyancy, the x, y and z terms are elements of the $\mathbf{r}$ vector, and represents the position of the body-fixed reference frame given in the

inertial reference frame, and the angles θ and ϕ are elements of η which is a vector of Euler angles between the body-fixed and inertial reference frame.

3.1.2.1 Added Mass

In hydrodynamics it is common to assume that the hydrodynamic forces and moments on a rigid body can be superimposed into the following equation:

$$\boldsymbol{\tau}_{hyd} = -\mathbf{M}_A\dot{\boldsymbol{\nu}}_r - \mathbf{C}_A(\boldsymbol{\nu}_r)\boldsymbol{\nu}_r - \mathbf{D}(\boldsymbol{\nu}_r)\boldsymbol{\nu}_r. \tag{3.10}$$

$\mathbf{M}_A$ is the added mass matrix, $\mathbf{C}_A$ is the Coriolis and centripetal added mass matrix and $\mathbf{D}$ is the hydrodynamic damping matrix. The nonlinear Coriolis and centripetal added mass matrix is due to the rotation of the body-fixed frame relative to the inertial reference frame, and can be derived using an energy formulation based on the constant added mass matrix, $\mathbf{M}_A$. Whcih can be written in matrix form as following:

$$\mathbf{M}_A = -\begin{bmatrix} X_{\dot{u}}u & X_{\dot{v}}v & X_{\dot{w}}w & X_{\dot{p}}p & X_{\dot{q}}q & X_{\dot{r}}r \\ Y_{\dot{u}}u & Y_{\dot{v}}v & Y_{\dot{w}}w & Y_{\dot{p}}p & Y_{\dot{q}}q & Y_{\dot{r}}r \\ Z_{\dot{u}}u & Z_{\dot{v}}v & Z_{\dot{w}}w & Z_{\dot{p}}p & Z_{\dot{q}}q & Z_{\dot{r}}r \\ K_{\dot{u}}u & K_{\dot{v}}v & K_{\dot{w}}w & K_{\dot{p}}p & K_{\dot{q}}q & K_{\dot{r}}r \\ M_{\dot{u}}u & M_{\dot{v}}v & M_{\dot{w}}w & M_{\dot{p}}p & M_{\dot{q}}q & M_{\dot{r}}r \\ N_{\dot{u}}u & N_{\dot{v}}v & N_{\dot{w}}w & N_{\dot{p}}p & N_{\dot{q}}q & N_{\dot{r}}r \end{bmatrix} \tag{3.11}$$

Since any motion of the vessel induces motion to a motion less fluid, the fluid must move aside and then close behind the vessel in order to let it move through the fluid. As a consequence, the fluid now possesses kinematic energy it else would not have. By using Kirchoff's equation one can derive the Coriolis and centripetal added mass matrix. For a rigid body moving through an ideal fluid the hydrodynamic Coriolis and centripetal matrix can always be parameterized so it is always skew-symmetric (Fossen 2011). Such a parametrization is:

$$\mathbf{C}_A(\boldsymbol{\nu}) = \begin{bmatrix} \mathbf{0}_{3\times3} & -\mathbf{S}(\mathbf{A}_{11}\boldsymbol{\nu}_1 + \mathbf{A}_{12}\boldsymbol{\nu}_2) \\ -\mathbf{S}(\mathbf{A}_{11}\boldsymbol{\nu}_1 + \mathbf{A}_{12}\boldsymbol{\nu}_2) & -\mathbf{S}(\mathbf{A}_{21}\boldsymbol{\nu}_1 + \mathbf{A}_{22}\boldsymbol{\nu}_2) \end{bmatrix} \tag{3.12}$$

$\mathbf{S}$ denotes the cross product operator, and the $\mathbf{A}_{ij}$ terms are given by:

$$\mathbf{M}_A = \begin{bmatrix} \mathbf{A}_{11} & \mathbf{A}_{12} \\ \mathbf{A}_{21} & \mathbf{A}_{22} \end{bmatrix} \tag{3.13}$$

Furthermore, $\mathbf{C_A}(\nu)$ can be written in component form according to:

$$\mathbf{C_A}(\boldsymbol{\nu}) = \begin{bmatrix} 0 & 0 & 0 & 0 & -a_3 & a_2 \\ 0 & 0 & 0 & a_3 & 0 & -a_1 \\ 0 & 0 & 0 & -a_2 & a_1 & 0 \\ 0 & -a_3 & a_2 & 0 & -b_3 & b_2 \\ a_3 & 0 & -a_1 & b_3 & 0 & -b_1 \\ -a_2 & a_1 & 0 & -b_2 & b_1 & 0 \end{bmatrix} \tag{3.14}$$

Where the components represents the following:

$$a_1 = X_{\dot{u}}u + X_{\dot{v}}v + X_{\dot{w}}w + X_{\dot{p}}p + X_{\dot{q}}q + X_{\dot{r}}r \tag{3.15}$$
$$a_2 = Y_{\dot{u}}u + Y_{\dot{v}}v + Y_{\dot{w}}w + Y_{\dot{p}}p + Y_{\dot{q}}q + Y_{\dot{r}}r \tag{3.16}$$
$$a_3 = Z_{\dot{u}}u + Z_{\dot{v}}v + Z_{\dot{w}}w + Z_{\dot{p}}p + Z_{\dot{q}}q + Z_{\dot{r}}r \tag{3.17}$$
$$a_4 = K_{\dot{u}}u + K_{\dot{v}}v + K_{\dot{w}}w + K_{\dot{p}}p + K_{\dot{q}}q + K_{\dot{r}}r \tag{3.18}$$
$$a_5 = M_{\dot{u}}u + M_{\dot{v}}v + M_{\dot{w}}w + M_{\dot{p}}p + M_{\dot{q}}q + M_{\dot{r}}r \tag{3.19}$$
$$a_6 = N_{\dot{u}}u + N_{\dot{v}}v + N_{\dot{w}}w + N_{\dot{p}}p + N_{\dot{q}}q + N_{\dot{r}}r \tag{3.20}$$

3.1.2.2 Damping

The main contributors to the hydrodynamic damping, $\mathbf{D}(\boldsymbol{\nu}_r)\boldsymbol{\nu}_r$ are:

- **Skin friction:** Linear frequency-dependent skin friction is due to laminar boundary layer, while nonlinear skin friction is due to turbulent boundary layer.
- **Damping Due to Vortex Shedding:** *D'Alambert's paradox* states that no hydrodynamic forces act on a fully submerged body with constant velocity in a nonviscous fluid. However, in a viscous fluid, frictional forces are present so that the system is no conservative with respect to energy. This is referred to as *interference drag*. It is a result of vortex shedding at sharp edges (Fossen 2011).

The expression for interference drag, also recognized as one of the terms in *Morison's equation*, is:

$$F(u) = -\frac{1}{2}\rho C_D(R_N)A|u|u \tag{3.21}$$

where ρ is the water density, $C_D(R_N)$ is the drag coefficient as a function of the Reynolds number, A is the projected area relative to the flow and u is the flow velocity (Eidsvik 2018). Equation 3.21 shows that the drag terms contribute to both linear and quadratic damping. Due to difficulties of separating these terms, even though experiments shows that the total drag force on a submerged vehicle can be appropriately described by the sum of a linear and quadratic drag component, the hydrodynamic damping can now be described by:

$$\mathbf{D}(\boldsymbol{\nu}_r)\boldsymbol{\nu}_r = \mathbf{D_L}\boldsymbol{\nu}_r + \mathbf{D_Q}\boldsymbol{\nu}_r|\boldsymbol{\nu}_r| \tag{3.22}$$

The linear damping matrix, with decoupled surge dynamics, can be written as:

$$\mathbf{D}_L = \begin{bmatrix} X_u & 0 & 0 & 0 & 0 & 0 \\ 0 & Y_v & 0 & Y_p & 0 & Y_r \\ 0 & 0 & Z_w & 0 & Z_q & 0 \\ 0 & K_v & 0 & K_p & 0 & K_r \\ 0 & 0 & M_w & 0 & M_q & 0 \\ 0 & N_v & 0 & N_p & 0 & N_r \end{bmatrix} \tag{3.23}$$

where the diagonal terms are given by:

$$-X_u = B_{11v} = \frac{m + A_{11}(0)}{T_{surge}} \tag{3.24}$$

$$-Y_v = B_{22v} = \frac{m + A_{22}(0)}{T_{sway}} \tag{3.25}$$

$$-Z_w = B_{33v} + B_{33}(\omega_{heave}) = 2\Delta\zeta_{heave}\omega_{heave}[m + A_{33}(\omega_{heave})] \tag{3.26}$$

$$-K_P = B_{44v} + B_{44} + B_{44}(\omega_{roll}) = 2\Delta\zeta_{roll}\omega_{roll}[I_x + A_{44}(\omega_{roll})] \tag{3.27}$$

$$-M_q = B_{55v} + B_{55}(\omega_{pitch}) = 2\Delta\zeta_{pitch}\omega_{pitch}[I_y + A_{55}(\omega_{pitch})] \tag{3.28}$$

$$-N_r = B_{66v} = \frac{I_z + A_{66}(0)}{T_{yaw}} \tag{3.29}$$

For ROV the damping matrices can be simplified into diagonal matrices. This is because these are the terms that dominates, and it is difficult and time consuming to determine the off diagonal parameters. Since these often contributes to negligible effects, it is common set them to zero. The damping equation is strictly positive since it describes energy being removed from the system.

3.1.2.3 Combined Model

The total equation of motion can be written as:

$$(\mathbf{M}_{RB} + \mathbf{M}_A)\dot{\boldsymbol{\nu}} + (\mathbf{C}_{RB}(\boldsymbol{\nu}_r) + \mathbf{C}_A(\boldsymbol{\nu}_r))\boldsymbol{\nu}_r + \mathbf{D_L}\boldsymbol{\nu}_r + \mathbf{D_Q}\boldsymbol{\nu}_r|\boldsymbol{\nu}_r| + \mathbf{g}(\boldsymbol{\eta}) = \boldsymbol{\tau} \quad (3.30)$$

In order to make this an appropriate model of the real physical system, all the matrices need to be accurately estimated. The mass, Coriolis and centripetal, and damping matrices are of dimensions 6×6, while the hydrostatic and thruster forces and moments are 6-by-1 vectors. After the equation of motion is derived, the rest becomes a matter of deriving the matrices and vector in order to correctly model the ROV system. This is costly, time consuming and complex. In order to determine the parameters, assumptions are used to simplify the complex system. Together with the necessity of performing experiments, this can produce inaccurate results because of measurements errors, flaws in experimental setup and simplifications of the system.

Chapter 4

Manipulator Kinematics

A robotic manipulator is a collection of rigid bodies whose relative motion is constrained by admissible velocities of the joints connecting two consecutive rigid bodies in the system. (From 2014). The joint motion is often very simple one degree of freedom linear or rotational motion. Manipulator systems therefore consists of either revolute or prismatic joints or a combinations of these. The manipulator system considered in this thesis, Orion 7P, shown in Figure 4.1, is built up by revolute joints. This gives very favorable characteristics to the robot's workspace, and it makes the modelling a lot easier, as the homogeneous transformation matrices can be written in a very simple form.

Figure 4.1: Manipulator system, Orion 7R

The Orion manipulator system is a compact, lightweight series, suitable for light, and medium-class ROVs. All of its segments are fabricated from hard-anodized extruded aluminium, which provides strength and corrosion resistance. It is a 7 degree of freedom system, consisting solely of revolute joints. The position sensors are magnetically

coupled and sealed in laser welded titanium housings ensuring protection. Some of the design parameters, properties and limitations can be seen in Table 1.1 and Table 1.2.

4.1 Kinematics

In robotics there are two types of kinematics, direct kinematics and inverse kinematics. In the direct kinematics the end-effector orientation is calculated by knowing the joint angles. In inverse kinematics, the end-effector position and orientation is given, and then the needed joint angles to make this possible are calculated.

The configuration of a body frame $\{b\}$ can be represented in the fixed space frame $\{s\}$ by specifying the position p of the frame $\{b\}$ in $\{s\}$ coordinates. This type of configuration is given by the homogeneous transformation matrix, $\mathbf{T}$, given by

$$\mathbf{T} = \left[\begin{array}{c|c} \mathbf{R}_{3\times3} & \mathbf{P}_{3\times1} \\ \hline 0_{1\times3} & 1 \end{array}\right] = \begin{bmatrix} r_{11} & r_{12} & r_{13} & P_1 \\ r_{21} & r_{22} & r_{23} & P_2 \\ r_{31} & r_{32} & r_{33} & P_3 \\ 0 & 0 & 0 & 1 \end{bmatrix} \tag{4.1}$$

4.1.1 Denavit Hartenberg Convention

When assigning the reference frames for each of the mnaipulator links, the Denavit-Hartenberg(DH) convention is used. This convention assumes that joints can be modeled as ideal revolute joints and that the joints are fixed relative to their associated links. Any robotic manipulator can be described kinematically by giving the values of four quantities for each link. Two describe the link itself, while the two other describe the link's connection to the neighbouring link. The four parameters are (Spong 2006):

- a_i - **Link length:** Distance from z_i to z_{i+1} along x_i.
- α_i - **Link twist:** Angle from z_i to z_{i+1} about x_i.
- d_i - **Link offset:** Distance between x_{i-1} to x_i along z_i.
- θ_i - **Joint angle:** Angle from x_{i-1} to x_i about z_i.

By following this convention, coordinate frames are attached to the joints connecting different links, and each homogeneous transformation between the frames is represented as a product of four basic transformations, also known as the link transformation.

$$\mathbf{A}_i = Rot_{z,\theta_i} Trans_{z,d_i} Trans_{x,a_i} Rot_{x,\alpha_i} \tag{4.2}$$

$$= \begin{bmatrix} c_{\theta_i} & -s_{\theta_i} & 0 & 0 \\ s_{\theta_i} & c_{\theta_i} & 0 & 0 \\ 0 & 0 & 1 & 0 \\ 0 & 0 & 0 & 1 \end{bmatrix} \begin{bmatrix} 1 & 0 & 0 & 0 \\ 0 & 1 & 0 & 0 \\ 0 & 0 & 1 & d_i \\ 0 & 0 & 0 & 1 \end{bmatrix} \begin{bmatrix} 1 & 0 & 0 & a_i \\ 0 & 1 & 0 & 0 \\ 0 & 0 & 1 & 0 \\ 0 & 0 & 0 & 1 \end{bmatrix} \begin{bmatrix} 1 & 0 & 0 & 0 \\ 0 & c_{\alpha_i} & -s_{\alpha_i} & 0 \\ 0 & s_{\alpha_i} & c_{\alpha_i} & 0 \\ 0 & 0 & 0 & 1 \end{bmatrix} \tag{4.3}$$

$$= \begin{bmatrix} c_{\theta_i} & -s_{\theta_i} c_{\alpha_i} & s_{\theta_i} s_{\alpha_i} & a_i c_{\theta_i} \\ s_{\theta_i} & c_{\theta_i} c_{\alpha_i} & -c_{\theta_i} s_{\alpha_i} & a_i s_{\theta_i} \\ 0 & s_{\alpha_i} & c_{\alpha_i} & d_i \\ 0 & 0 & 0 & 1 \end{bmatrix} \tag{4.4}$$

The matrix, $\mathbf{A}_i$, is a function of one variable, hence three of four quantities are constant. For revolute joints θ_i is the variable, while d_i is the variable for prismatic joints. It is not possible to represent any arbitrary homogeneous transformation using only four parameters. Therefore, the possible homogeneous transformations in the form of 4.2 need to be expressed. Given two frames, denoted 0 and 1, seen in Figure 4.2, satisfying the following DH assumptions:

- The axis x_1 is perpendicular to the axis z_0.
- The axis x_i intersects the axis z_0.

then there exist a unique homogeneous transformation matrix A that transforms the coordinates of frame 1 into frame 0.

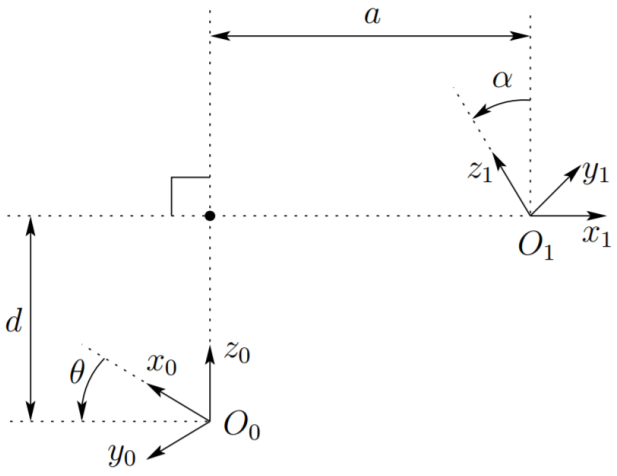

Figure 4.2: Coordinate frames satisfying the DH assumptions

To be able to find all these parameters, all the axis of the system needs to be defined. Figure 4.3 shows how the reference frames of each joint and module is defined, in order to determine the DH-parameters and the transformation matrices.

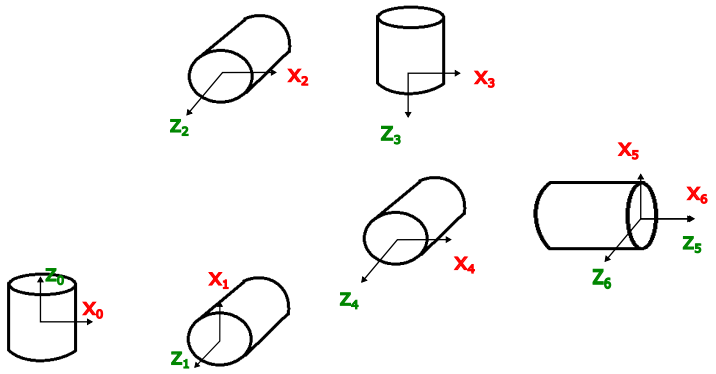

Figure 4.3: Schematic representation of the coordinate-axes used to determine DH parameters and homogeneous transformation matrices

With this setup of the reference frames, the obtained Denavit-Hartenberg parameters are shown in Table 4.1.

Table 4.1: Denavit-Hartenberg Parameters

i	$\alpha_i[rad]$	$a_i[mm]$	$d_i[mm]$	$\theta_i[rad]$
1	$\frac{\pi}{2}$	64.9	0	θ_1
2	0	957.1	0	$\theta_2 + \frac{\pi}{2}$
3	$\frac{\pi}{2}$	125	0	$\theta_3 - \frac{\pi}{2}$
4	$-\frac{\pi}{2}$	0	580	θ_4
5	$-\frac{\pi}{2}$	259	0	θ_5
6	$-\frac{\pi}{2}$	0	0	θ_6

4.1.2 Direct Kinematics

When the Denavit-Hartenberg parameters and the transformation matrix are determined, the position of the end-effector can be calculated, given the joint angles. The transformation between the base-frame and the end-effector frame is done by finding the transformation between each adjacent reference-frame, $\mathbf{T}_0^1$, $\mathbf{T}_1^2$, $\mathbf{T}_2^3 \dots \mathbf{T}_7^8$, then multiplying these together. Each of these transformations are found by Equation 4.5.

$$\mathbf{T}_{i-1}\hat{\mathrm{i}} = \begin{bmatrix} c_{\theta_i} & -s_{\theta_i}c_{\alpha_i} & s_{\theta_i}s_{\alpha_i} & a_i c_{\theta_i} \\ s_{\theta_i} & c_{\theta_i}c_{\alpha_i} & -c_{\theta_i}s_{\alpha_i} & a_i s_{\theta_i} \\ 0 & s_{\alpha_i} & c_{\alpha_i} & d_i \\ 0 & 0 & 0 & 1 \end{bmatrix} \in \mathbb{R}^{6\times 6} \quad (4.5)$$

The transformation from the base-frame to the end-effector reference-frame is then calculated using Equation **??**

$$\mathbf{T}_0^6 = \mathbf{T}_0^1 * \mathbf{T}_1^2 * \mathbf{T}_2^3 * \mathbf{T}_3^4 * \mathbf{T}_4^5 * \mathbf{T}_5^6 \quad (4.6)$$

A point, $\mathbf{P}$ in the body frame, b, for instance the position of the end-effector, can be represented in the fixed base frame, s, through

$$\begin{bmatrix} \mathbf{P}^{\{b\}} \\ 1 \end{bmatrix} = \mathbf{T}_{\{s\}}^{\{b\}} \begin{bmatrix} \mathbf{P}^{\{s\}} \\ 1 \end{bmatrix} \quad (4.7)$$

After the position is calculated, the Euler angles, α, β and γ, needs to be determined. These are computed according to Equation (4.8)-(4.10)

$$\beta = atan2(-\sqrt{r_{13}^2 + r_{23}^2}, r_{33}) \quad (4.8)$$

$$\alpha = atan2(\pm r_{23}, \pm r_{13}) \quad (4.9)$$

$$\gamma = atan2(\pm r_{32}, \mp r_{31}) \quad (4.10)$$

The signs of the rotation terms in the expression for α and γ, is dependent on whether β is positive or negative. These calculations are carried out with the assumption that every position within the manipulators reach is possible. In other words, there are no mechanical constraints.

There are mainly two important interpretations of the homogeneous transformation matrix. Firstly, when the transformation between two coordinate frames is known, any quantity calculated in one coordinate frame can be transformed to the other by simple matrix multiplication. Secondly, we can describe how a reference frames moves in space as a time-varying homogeneous transformation matrix. This matrix therefore gives us the time evolution of a rigid body in space as observed from a single reference frame (From 2014).

4.1.3 Inverse Kinematics

Inverse kinematics is the determination of joint variables given the end-effector position and orientation. The solution of the inverse kinematic problem is of fundamental importance in order to transform the motion, assigned to end-effector in the operational space, into the corresponding joint space motion that allows execution of the desired motion.

Compared to direct kinematics, the inverse kinematics is a much more complex problem, because of the following reasons (Siciliano et al. 2009):

- The equations to solve are in general nonlinear, and thus it is not always possible to find a closed-form solution
- Multiple solution may exist.
- Infinite solutions may exist, for instance in the case of a kinematically redundant manipulator.
- There might be no admissible solution, in view of the manipulator kinematic structure.

There are different methods applicable in order to solve the inverse kinematics problem, and in this thesis the geometric method and algebraic method is used.

4.1.3.1 Solvability

Solving the inverse kinematic is a nonlinear problem, and as for any nonlinear problem, or set of equations, the existence of solutions must be of concern. The question of whether any solution exists is often answered by inspecting the workspace. The workspace is the volume of spasce which the end-effector can reach. For a solution to exist the specified point must lie withing the workspace. Often, the workspace is considered by two different definitions, dextrous and reachable workspace. Dextrous workspace is that volume of space that the robot end-effector can reach with all orientations. Meaning, that at each point in the dextrous workspace the end-effector can be arbitrarily oriented. The reachable workspace is that volume of space that the robot can reach in at least one orientation (Craig 1989).

A possible problem within the inverse kinematics, is the existence of multiple solutions. For instance, consider a three link manipulator as shown in Figure 4.4.

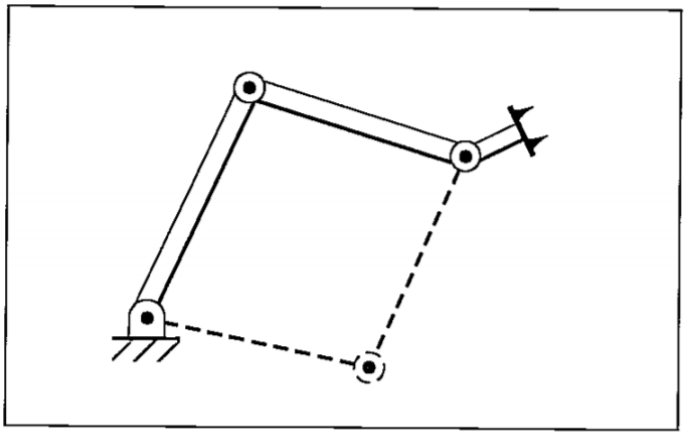

Figure 4.4: Three link manipulator

A planar arm with three revolute joints has a large dextrous workspace, because the a position within the workspace can be reached with any orientation. As seen from this Figure, the end-effector position can be reached in two different configurations. The second joint can be placed in two different positions, where the dashed line represents the second solution. The fact that the manipulator can reach the same position with different configurations, can cause problem since it has to chose a solution. A criteria applicable here, is to chose to closest configuration solution to the current configuration. This type of criteria is shown in Figure 4.5.

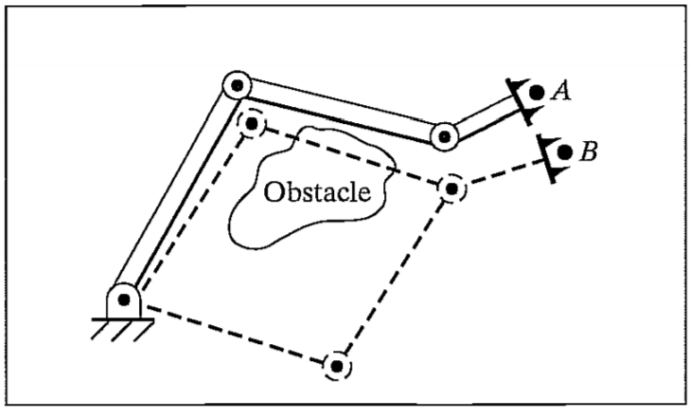

Figure 4.5: Three link manipulator with two solutions

If the current position of the end-effector is at point A, then the most logically solution to reach point B is to chose the configuration as shown in the figure, rather than the solution the dashed line represents.

The number of soltion is dependent on the number of joints in the manipulator but also the link parameters, $\alpha_{i-1}, a_{i-1} and d_i$ from the Denavit-Hartenberg convention, and the ranges of motion of the joints.

4.1.3.2 Geometric method

This method is based on using basic trigonometric relations and planar geometry in order to calculate the joint angles. To use this method it is common to divide the manipulator into several plane-geometry problems, where joints that only works in a 2D-plane is considered.

If a joint is rotatable so if enables the next joint to operate in all 3 dimensions, a trigonometric approach will, more often than not, be insufficient. In order to solve such a problem, the algebraic method can be utilized.

4.1.3.3 Algebraic method

The algebraic method is a method that calculates the joint angles by solving the following equation:

$$\underbrace{\begin{bmatrix} r_{11} & r_{12} & r_{13} & p_x \\ r_{21} & r_{22} & r_{23} & p_y \\ r_{31} & r_{32} & r_{33} & p_z \end{bmatrix}}_{{}^{tool}_{base}T} = \mathbf{T}_0^1(\theta_1) * \mathbf{T}_1^2 * \mathbf{T}_2^3(\theta_2) * \mathbf{T}_3^4(\theta_3) * \mathbf{T}_4^5(\theta_4) * \mathbf{T}_5^6 * \mathbf{T}_6^7(\theta_5) * \mathbf{T}_7^8(\theta_6) \quad (4.11)$$

where ${}^{tool}_{base}T$ is a given homogeneous link transformation and $\theta_1 \dots \theta_6$ are the unknown joint angles.

This method often follow the following procedure:

$$\mathbf{T}_7^8(\theta_6) = [\mathbf{T}_0^1(\theta_1) * \mathbf{T}_1^2 * \mathbf{T}_2^3(\theta_2) * \mathbf{T}_3^4(\theta_3) * \mathbf{T}_4^5(\theta_4) * \mathbf{T}_5^6 * \mathbf{T}_6^7(\theta_5)]^{-1} {}^{tool}_{base}\mathbf{T} \quad (4.12)$$

$$\mathbf{T}_6^7(\theta_5) * \mathbf{T}_7^8(\theta_6) = [\mathbf{T}_0^1(\theta_1) * \mathbf{T}_1^2 * \mathbf{T}_2^3(\theta_2) * \mathbf{T}_3^4(\theta_3) * \mathbf{T}_4^5(\theta_4) * \mathbf{T}_5^6]^{-1} {}^{tool}_{base}\mathbf{T} \quad (4.13)$$

$$\mathbf{T}_5^6 * \mathbf{T}_6^7(\theta_5) * \mathbf{T}_7^8(\theta_6) = [\mathbf{T}_0^1(\theta_1) * \mathbf{T}_1^2 * \mathbf{T}_2^3(\theta_2) * \mathbf{T}_3^4(\theta_3) * \mathbf{T}_4^5(\theta_4)]^{-1} {}^{tool}_{base}\mathbf{T} \quad (4.14)$$

$$\vdots \quad (4.15)$$

$$\mathbf{T}_1^2 * \cdots * \mathbf{T}_6^7(\theta_5) = [\mathbf{T}_0^1(\theta_1)]^{-1} {}^{tool}_{base}\mathbf{T} \quad (4.16)$$

Since one or more joint angles are already determined from the geometric method, several steps in this procedure can often be ignored. To solve each of the equations only one slot of each matrix needs to equal to each other. By inspecting the left hand side matrix and the right hand side matrix, one can choose the combination which gives the easiest solvable equation. In other words, the algebraic method is basically manipulating the given equations into a form for which a solution is known.

4.2 Twists

The notion of twists provides a compact way of representing the relative velocity of a reference frame with respect to another. The twist $\mathbf{V}$ can be written as

$$\mathbf{V_{ab}} := [\boldsymbol{v}_{ab}^T \quad \boldsymbol{\omega}_{\boldsymbol{ab}}^{\boldsymbol{T}}] \tag{4.17}$$

where $\upsilon_{\mathbf{ab}}$ and $\omega_{\mathbf{ab}}$ represents the linear and angular velocity of frame $\mathcal{F}_b$ relative to frame $\mathcal{F}_a$. Often, the twist are categorized as *body twist* or *spatial twist*. For body twist, the relative velocity, $\mathbf{V_{ab}}$, is written as seen from $\mathcal{F}_b$, while for spatial twist, according to (From 2014), the linear part of the spatial velocity of a rigid body relative to a reference frame is the velocity of a point attached to a possible imaginary extension of the body, moving through the reference frame. To avoid ambiguity, the body is twist is denoted with a superscript B, $\mathbf{V_{ab}^B}$, and the spatial twist is denoted with a superscript S, $\mathbf{V_{ab}^S}$.

The spatial twist is often used to derive the velocity kinematics, therefore, a mapping between body twist and spatial twist is practical. The *adjoint transformation* associated with the homogeneous transformation matrix, is such a mapping. This transformation is represented by the matrix $\mathbf{Ad_{T_b}}$, which is defined as

$$\mathbf{Ad_{T_{ab}}} := \begin{bmatrix} \mathbf{R_{ab}} & \widehat{\mathbf{p}}_{\mathbf{ab}}\mathbf{R_{ab}} \\ 0 & \mathbf{R_{ab}} \end{bmatrix} \in \mathbb{R}^{6\times 6} \tag{4.18}$$

$$\mathbf{Ad_{T_{ab}}^{-1}} := \begin{bmatrix} \mathbf{R_{ab}}^T & -\mathbf{R_{ab}^T}\widehat{\mathbf{p}}_{\mathbf{ab}} \\ 0 & \mathbf{R_{ab}^T} \end{bmatrix} \in \mathbb{R}^{6\times 6} \tag{4.19}$$

where $\mathbf{R_{ab}}$ is the rotation matrix from frame a to b, and $\widehat{\mathbf{p}}_{\mathbf{ab}}$ maps the position vector into its skew-symmetric matrix representation, which is defined as

$$\widehat{\mathbf{p}} = \begin{bmatrix} 0 & -p_3 & p_2 \\ p_3 & 0 & -p_1 \\ -p_2 & p_1 & 0 \end{bmatrix} \tag{4.20}$$

The mapping of body twist into spatial twist is done accordingly

$$\mathbf{V_{ab}^S} = \mathbf{Ad_{T_{ab}}}\mathbf{V_{ab}^B} \tag{4.21}$$

Some important properties of the adjoint transformation matrix are (Murray 1994)

$$\mathbf{Ad_{ac}} = \mathbf{Ad_{ab}}\mathbf{Ad_{bc}} \tag{4.22}$$
$$\mathbf{Ad_{ac}^{-1}} = \mathbf{Ad_{ca}} \tag{4.23}$$

Further on, (Murray 1994) states that if we let $\mathcal{F}_c$ and $\mathcal{F}_d$ be attached to the same rigid body and let $\mathbf{V_{0c}}$ and $\mathbf{V_{0d}}$ be their respective body velocities, then we can use adjoint transformation matrix to map between the two

$$\mathbf{V_{0c}} = \mathbf{Ad_{T_{cd}}}\mathbf{V_{0d}} \tag{4.24}$$

This is proved by starting with the following

$$\mathbf{V_{0c}^S} = \mathbf{Ad_{T_{0c}}}\mathbf{V_{0c}} \tag{4.25}$$
$$\mathbf{V_{0d}^S} = \mathbf{Ad_{T_{0d}}}\mathbf{V_{0d}} \tag{4.26}$$

Since the spatial twist is not dependent on a specific frame on the rigid body, we have that

$$\mathbf{V_{0c}^S} = \mathbf{V_{0d}^S} \tag{4.27}$$

Then we can substitute equation (4.25) and (4.26) and retrieve

$$\mathbf{Ad_{T_{0c}}}\mathbf{V_{0c}^S} = \mathbf{Ad_{T_{0d}}}\mathbf{V_{0d}^S} \tag{4.28}$$
$$\mathbf{V_{0c}^S} = \mathbf{Ad_{T_{0c}}^{-1}}\mathbf{Ad_{T_{0d}}}\mathbf{V_{0d}^S} \tag{4.29}$$
$$\mathbf{V_{0c}^S} = \mathbf{Ad_{T_{c0}}}\mathbf{Ad_{T_{0d}}}\mathbf{V_{0d}^S} \tag{4.30}$$
$$\mathbf{V_{0c}^S} = \mathbf{Ad_{T_{cd}}}\mathbf{V_{0d}^S} \tag{4.31}$$

4.3 Static Forces and Moments in the Manipulator

When the manipulator is in contact with the surrounded environment, contact forces is applied to the end-effector. These forces then creates forces and moments in joints, which propagates all the way through to the base of the manipulator. These forces and moments affects the behaviour of both the manipulator and the base to which it is mounted on. To be able to control either the manipulator itself or the vehicle it is mounted on, it is important to calculate these.

4.3.1 Jacobian Matrix

The Jacobian matrix is a multidimensional form of the derivative, and is often used to map the dynamic relationship between the joints in a manipulator, i.e. how movement in one joint causes other joints also to move. Additionally, it can be used to calculate the magnitude of the torque occurring at the joints. The Jacobian is usually defined as shown in Equation (4.32).

$$\boldsymbol{\nu} = \mathbf{J}(\mathbf{q})\dot{\mathbf{q}} \tag{4.32}$$

where $\boldsymbol{\nu}$ is the 6x1 Cartesian velocity vector of the end-effector, $\mathbf{J}$ 4 is the Jacobian matrix and q is the vector of the manipulator joint angles. The velocity vector contains both linear and angular velocity, such as

$$\boldsymbol{\nu} = \begin{bmatrix} \boldsymbol{\nu} \\ \boldsymbol{\omega} \end{bmatrix}. \tag{4.33}$$

The number of rows in the Jacobian matrix equals the number of states in the velocity vector, while the number of columns is dependent on the number of joints in the manipulator. Various methods can be used to calculate the Jacobian matrix. By partial differentiating the kinematic equations of the mechanism with respect to the joint angles, the Jacobian is found. Anther method, is by utilizing the table in Figure 4.2.

Table 4.2: Calculate the Jacobian

	Prismatic	Revolute	
Linear	$\mathbf{R}^0_{i-1}\begin{bmatrix}0\\0\\1\end{bmatrix}$	$\mathbf{R}^0_{i-1}\begin{bmatrix}0\\0\\1\end{bmatrix}$	$\times(\mathbf{d}^0_n - \mathbf{d}^0_{i-1})$
Rotational	$\begin{bmatrix}0\\0\\0\end{bmatrix}$	$\mathbf{R}^0_{i-1}\begin{bmatrix}0\\0\\1\end{bmatrix}$	

Here, $\mathbf{R}^0_{i-1}$ is the rotation matrix from frame $\{0\}$ to frame $\{i-1\}$, $\mathbf{d}^0_n$ is the displacement vector from frame $\{0\}$ to frame $\{n\}$ (n is the number of joints), $\mathbf{d}^0_{i-1}$ is the displacement vector from frame $\{0\}$ to frame $\{i-1\}$.

Singularities When operating with Jacobian matrices to either calculate velocities or forces, properties such as invertibility needs to be considered. Which also means,m if the matrix is nonsingular. If the matrix is nonsingular, we can calculate joint rates from the Cartesian velocities by inverting the Jacobian matrix:

$$\dot{\mathbf{q}} = \mathbf{J}^{-1}(\mathbf{q})\boldsymbol{\nu} \tag{4.34}$$

Most manipulators has values of $\mathbf{q}$, which makes the Jacobian matrix singular. Then it is not possible to invert it, ans these locations are singularities. All manipulators have singularities at the boundary of their workspace, but also within the workspace.

Workspace-boundary singularities occurs when the manipulator is either at its maximum reach, i.e. fully stretched, or folded back on itself in such a way that the end-effector is at its boundary of the workspace. These can be easily avoided by not driving the manipulator to the border of its workspace.

Internal singularities occurs inside the reachable workspace and are generally caused by alignment of two or more axes of motion, or by attainment of particular end-effector configurations. These singularities is of greater concern, as they can be encountered anywhere in the workspace for planned path in the operational space.

4.3.2 Joint Torques

Calculating the torques at the joints, can be done by the following equation:

$$\boldsymbol{\tau} = \mathbf{J}^T\boldsymbol{\mathcal{F}} \tag{4.35}$$

$\boldsymbol{\tau}$ is a vector of torques at the joints, $\boldsymbol{\mathcal{F}}$ is the force-moment vector acting on the end-effector and J is the Jacobian matrix. This relation allows us to convert Cartesian quantities into joint-space quantities without performing any inverse kinematics functions, which generally is very useful in robotics. When the Jacobian loses full rank, there are certain directions in which the end-effector cannot exert static forces even if desired. That is, if the Jacobian becomes singular, $\boldsymbol{\mathcal{F}}$ could be increased or decreased in certain directions without affecting the calculated joint torques values for $\boldsymbol{\tau}$. This means that near singular configurations, mechanical advantage tends toward infinity, such that small joint torques generates large forces at the end-effector (Craig 1989).

4.3.3 Force Propagation

Manipulator's design and configuration makes it quite trivial to figure out how forces and moments propagate through the chainlike nature. When it acts on the environment, forces are created at the end-effector. These forces will propagate through the links of the manipulator, and create moments in the joints, which also affects the vehicle it is

mounted on. It is therefore important to address how the different forces acts in and on the manipulator, in order to model its affection on the vehicle.

When considering static forces in a manipulator, all the joints are locked, in order to make it behave like a structure. Further on, each link is considered and force-moment balance relationship is derived. Finally, the static torque required to keep the joint in static equilibrium is calculated. The force equilibrium becomes:

$$f_i - f_{i+1} = 0 \tag{4.36}$$

where f_i is the force exerted on link i by link $i-1$. By summing the torques about the origin in frame i, this static equilibrium equation follows:

$$n_i - n_{i+1} - P_{i+1} \times f_{i+1} = 0 \tag{4.37}$$

where n_i is the torque exerted on link i by link $i-1$ and P_{i+1} is the distance between the origin of frame i to the origin of frame $i+1$. By starting the description of the force and moment applied to the manipulator at the last link, we can calculate the force and moment applied by each link down to the base, link 0. To describe these forces and moments in each link's reference frame, the rotation matrix relating frame $i+1$ to frame i is used. The propagation of forces and moments can therefore be described as following:

$$f_i =_{i+1}^{i} \mathbf{R}^{i+1} f_{i+1} \tag{4.38}$$

$$n_i =_{i+1}^{i} \mathbf{R}^{i+1} n_{i+1} + P_{i+1} \times f_i \tag{4.39}$$

Additionally to considering equilibrium at each, in order to determine the force propagation in the manipulator, one could transform the static forces and moments at the end-effector to the other link and joints by the use of the rotation matrices.

Cartesian Transformation of Static Forces The general force vector has a 6×1 representation, such as

$$\boldsymbol{\mathcal{F}} = \begin{bmatrix} \mathbf{F} \\ \mathbf{N} \end{bmatrix} \tag{4.40}$$

where $\mathbf{F}$ is a 3×1 force vector, and $\mathbf{N}$ is a 3×1 moment vector. Further on, we can introduce a 6×6 mapping operation that transform a force-moment vector in one frame to a force-moment vector in another frame. This way, we can calculate the force-moment vector at the base frame from the force-moment vector at the end-effector frame. The relationship is derived as following

$$\begin{bmatrix} {}^{A}\mathbf{F}_{A} \\ {}^{A}\mathbf{N}_{A} \end{bmatrix} = \begin{bmatrix} {}^{A}_{B}\mathbf{R} & \mathbf{0} \\ {}^{A}\mathbf{P}_{BORG} \times {}^{A}_{B}\mathbf{R} & {}^{A}_{B}\mathbf{R} \end{bmatrix} \begin{bmatrix} {}^{B}\mathbf{F}_{B} \\ {}^{B}\mathbf{N}_{B} \end{bmatrix} \tag{4.41}$$

${}^{A}_{B}R$ is the rotation matrix from fram B to frame A, and the cross product is understood as the matrix operator

$${}^{A}P_{BORG}\times = \begin{bmatrix} 0 & -p_x & p_y \\ p_x & 0 & -p_x \\ -p_y & p_x & 0 \end{bmatrix} \tag{4.42}$$

Equation 4.41 can be written more compactly as

$${}^{A}\mathbf{F}_{A} = {}^{A}_{B}\mathbf{T}_{f}\,{}^{B}\mathbf{F}_{B} \tag{4.43}$$

where ${}^{A}_{B}\mathbf{T}_{f}$ is used to denote a force-moment transformation (Craig 1989).

Chapter 5

Manipulator Dynamics

Manipulators with conventional prismatic or revolute joints are most efficiently modelled using an Lagrangian framework. Since the motion of the end-effector and the workspace of the manipulator are defined by the limitations of the joints, the Lagrangian framework is a natural choice of modelling method, because these constraints are included in the dynamics by choosing the generalized coordinates as the joints variables (From 2014).

5.1 Kinetic and Potential Energy in Multibody Systems

In order to carry out the Lagrangian modelling the total energy of the system needs to be known. The total energy is found by kinetic and potential energy of each rigid body with respect to a common inertial reference frame.

From equation (4.32) and 4.33,we know that the velocity vector of a link i, can be written on the form:

$$\mathbf{V}_{0i} = \begin{bmatrix} \boldsymbol{v}_{0i} \\ \boldsymbol{\omega}_{0i} \end{bmatrix} = \mathbf{J}_i(\mathbf{q})\dot{\mathbf{q}} \tag{5.1}$$

where v_{0i} and ω_{0i} are the linear and angular velocities, respectively, of link i, and J_i is the jacobian matrix. Thus, the velocities of the links are determined as long as the joint angles are known. From this, we can calculate the kinetic energy of each link

$$\begin{aligned}\mathcal{K}_i &= \frac{1}{2}(\mathbf{V}_{0i})^T\mathbf{I}_i\mathbf{V}_{0i} \\ &= \frac{1}{2}(\mathbf{Ad}_{T_{i0}}\mathbf{V}_{0i})^T\mathbf{I}_i\mathbf{Ad}_{T_{i0}}\mathbf{V}_{0i} \\ &= \frac{1}{2}(\mathbf{J}_i(\mathbf{q})\dot{\mathbf{q}})^T\mathbf{Ad}_{T_{i0}}^T\mathbf{I}_i\mathbf{Ad}_{T_{i0}}\mathbf{J}_i(\mathbf{q})\dot{\mathbf{q}} \\ &= \frac{1}{2}\dot{\mathbf{q}}^T\mathbf{J}_i(\mathbf{q})^T\mathbf{Ad}_{T_{i0}}^T\mathbf{I}_i\mathbf{Ad}_{T_{i0}}\mathbf{J}_i(\mathbf{q})\dot{\mathbf{q}} \\ &= \frac{1}{2}\dot{\mathbf{q}}_i^T\mathbf{M}_i(\mathbf{q})\dot{\mathbf{q}}_i \end{aligned} \tag{5.2}$$

$\mathbf{I}_i$ is the generalized inertial matrix and $\mathbf{Ad}_{T_{i0}}$ is the adjacent of the homogeneous transformation matrix. Since only Euclidean transformations are considered, we can rewrite equation (5.2) to

$$\mathcal{K}_\rangle = \frac{1}{2}\boldsymbol{\upsilon}_i^T\mathbf{M}_i(\mathbf{q})\boldsymbol{\upsilon}_i \tag{5.3}$$

Hence, we can see from equation (5.2) that the inertia matrix of link i can be expressed as:

$$\mathbf{M}_i(\mathbf{q}) = \mathbf{J}_i(\mathbf{q})^T\mathbf{Ad}_{T_{i0}}^T\mathbf{I}_i\mathbf{Ad}_{T_{i0}}\mathbf{J}_i(\mathbf{q}) \tag{5.4}$$

From this, the total kinetic energy of the manipulator can be calculated by summing the kinetic energy of each link (From 2014)

$$\mathcal{K}(\mathbf{q},\boldsymbol{\upsilon}) = \frac{1}{2}\boldsymbol{\upsilon}^T(\sum_{i=1}^{n}\mathbf{M}_i(\mathbf{q}))\boldsymbol{\upsilon} \tag{5.5}$$

The same procedure is used to determine the potential energy of the manipulator, i.e. first expressing the potential energy for each link, $\mathcal{U}_i$, and then take the sum of the potential energies. The potential energy of the system is related to the hydrostatic restoring force, and is found by

where $\mathbf{g_i}$ are the hydrostatic restoring forces and moments of link i and $[\eta_\mathbf{i}]_j$ denotes element j of the state vector $\eta_\mathbf{i}$ of joint i.

5.2 Equation of Motion

Now that the total energy of the system is found, we write the Lagrangian on the normal form as

$$\mathcal{L}(\mathbf{q}, \dot{\mathbf{q}}) = \mathcal{K}(\mathbf{q}, \dot{\mathbf{q}}) - \mathcal{U}(\mathbf{q}) \tag{5.6}$$

Then, the dynamics is found by the Lagrangian equation by

$$\frac{d}{dt}\left(\frac{\partial \mathcal{L}}{\partial \dot{q}_i}\right) - \frac{\partial \mathcal{L}}{\partial \mathbf{q_i}} = \boldsymbol{\tau} - \boldsymbol{\tau}_d - \boldsymbol{\tau}_{hs} \tag{5.7}$$

τ is the control torque of the joints, τ_d is the hydrodynamic drag forces and moments vector and τ_{hs} is the hydrostatic restoring forces and moments vector (Eidsvik 2018).

The partial derivatives of the Lagrangian equation are

$$\frac{d}{dt}\frac{\partial \mathcal{L}}{\partial \dot{\mathbf{q}}_i} = \frac{d}{dt}\left(\sum_{j=1}^{n} \mathbf{M}_{ij}(\mathbf{q})\dot{\mathbf{q}}_j\right) = \sum_{j=1}^{n}(\dot{\mathbf{M}}_{ij}(\mathbf{q})\dot{\mathbf{q}}_j + \mathbf{M}_{ij}(\mathbf{q})\ddot{\mathbf{q}}) \tag{5.8}$$

$$\frac{\partial \mathcal{L}}{\partial q_i} = \frac{1}{2}\sum_{j,k=1}^{n} \frac{\partial \mathbf{M}_{jk}(\mathbf{q})}{\partial \mathbf{q}_i}\dot{\mathbf{q}}_k\dot{\mathbf{q}}_j - \frac{\partial \mathcal{U}}{\partial \mathbf{q}_i} \tag{5.9}$$

By substituting (5.8) and (5.9) into the Lagrangian equation, we get

$$\sum_{j=1}^{n} \mathbf{M}_{ij}\ddot{\mathbf{q}}_j + \frac{1}{2}\sum_{j,k=1}^{n}\left(\frac{\partial \mathbf{M}_{ij}}{\partial \mathbf{q}_k}\dot{\mathbf{q}}_k\dot{\mathbf{q}}_j + \frac{\partial \mathbf{M}_{jk}}{\partial \mathbf{q}_j}\dot{\mathbf{q}}_k\dot{\mathbf{q}}_j - \frac{\partial \mathbf{M}_{jk}}{\partial \mathbf{q}_i}\dot{\mathbf{q}}_k\dot{\mathbf{q}}_j\right) + \frac{\partial \mathcal{U}}{\partial \mathbf{q}_i} = \boldsymbol{\tau}_i \tag{5.10}$$

The aim for the equation of motion for the manipulator is to be written in the same form as the equation of motion for the ROV, i.e. on matrix form. The dynamics of a serial manipulator can be written in terms of the generalized coordinates q, which are chosen as the joint positions, and generalized velocities, $\dot{q}$, which are joint velocities. This can be chosen for any manipulator consisting of 1-DOF revolute or prismatic joints. Further on, we can then write the manipulator dynamics in matrix form through the equation of motion

$$\mathbf{M}(\mathbf{q})\ddot{\mathbf{q}} + \mathbf{C}(\mathbf{q}, \dot{\mathbf{q}})\dot{\mathbf{q}} + \mathbf{N}(\mathbf{q}) = \boldsymbol{\tau} \tag{5.11}$$

Here $\mathbf{M}(\mathbf{q})$ is the manipulator inertia matrix, defined in equation (5.4), $\mathbf{C}(\mathbf{q}, \dot{\mathbf{q}})$ is the Coriolis matrix, $\mathbf{N}(\mathbf{q})$ is the potential force matrix. The Coriolis matrix is often expressed in terms of the Christoffel symbol, $\boldsymbol{\Gamma}$, as

$$\mathbf{C}_{ij}(\mathbf{q}, \dot{\mathbf{q}}) = \left\{\sum_{k=1}^{n} \boldsymbol{\Gamma}_{ijk}\dot{\mathbf{q}}_k\right\} \tag{5.12}$$

where Γ is foud by

$$\mathbf{\Gamma}_{ijk} = \frac{1}{2}\left(\frac{\partial \mathbf{M}_{ij}}{\partial \mathbf{q}_k} + \frac{\partial \mathbf{M}_{jk}}{\partial \mathbf{q}_j} - \frac{\partial \mathbf{M}_{jk}}{\partial \mathbf{q}_i}\right) \tag{5.13}$$

If gravitational forces are present, the potential forces, $N(q)$, needs to be included. The gravitational forces of each link, i, can be calculated as

$$\mathbf{F}_g^i = \begin{bmatrix} \mathbf{f}_i \\ \mathbf{r}_i^g \mathbf{f}_i \end{bmatrix} = -m_i g \begin{bmatrix} \mathbf{R}_{0i}\mathbf{e}_z \\ \mathbf{r}_i^g \mathbf{R}_{0i}\mathbf{e}_z \end{bmatrix} \tag{5.14}$$

where $\mathbf{R}_{0i}$ is the rotation matrix from the base frame to the body frame of link i, $\mathbf{e}_z = [001]^T$, $\mathbf{r}_i^g$ is the centre of gravity of link i expressed in the i'th reference frame and $\mathbf{f}_i$ represents the forces acting on link i at the centre of gravity. These gravitational forces creates joint torques, which also need to be calculated, This can be done by

$$\boldsymbol{\tau}_i^g = \mathbf{J}_i^T(\mathbf{q})\mathbf{Ad}_{T_{0i}}^T(\mathbf{q})\mathbf{F}_g^i(\mathbf{q}). \tag{5.15}$$

Equation (5.15) represents the joint torques in each of the joints associated with link i, therefore, in order to calculate the total effect of the gravitational forces, summing the effect of each link is done, which is shown in equation (5.16).

$$\mathbf{N}(\mathbf{q}) = \sum_{i=1}^{n} \boldsymbol{\tau}_i^g \tag{5.16}$$

Now that the dynamics of the ROV and the manipulator are defined, a model of which combines these two dynamics can be designed, called Underwater Vehicle-Manipulator Systems (UVMS).

Chapter 6

Dynamics of Underwater Vehicle-Manipulator System

In this chapter, the dynamics of the underwater vehicle-manipulator system is derived.

6.1 Dynamics

The dynamic equations of UVMS needs special considerations, because it includes a combinations of non-Euclidean configuration spaces and multibody systems. Therefore, models used for single rigid bodies or multibody systems with Euclidean configuration spaces cannot be applied, because it will not result in well defined dynamics of the system. In the previous sections, the dynamics of a single rigid body, the ROV, and a multibody system, the manipulator, have been presented, in this section the dynamics of these systems combined will be derived, in terms of quasi velocities.

For manipulators with Euclidean joints, the quasi velocity is equal to the generalized velocity, while for the rigid body it is given by its velocity vector. Therefore, the combined state space can be written as

$$\boldsymbol{\xi} = \begin{bmatrix} \boldsymbol{\eta} \\ \mathbf{q} \end{bmatrix} = \begin{bmatrix} x \\ y \\ z \\ \psi \\ \theta \\ \phi \\ q_1 \\ \vdots \\ q_n \end{bmatrix}, \qquad \boldsymbol{\zeta} = \begin{bmatrix} \mathbf{V}_{0b}^{B} \\ \dot{\mathbf{q}} \end{bmatrix} = \begin{bmatrix} u \\ v \\ w \\ p \\ q \\ r \\ \dot{q}_1 \\ \vdots \\ \dot{q}_n \end{bmatrix} \tag{6.1}$$

Since the dynamics of the UVMS are preferably on the same form as EOM of a rigid body and the manipulator, it should be written on the form

$$\dot{\boldsymbol{\xi}} = \mathbf{J}_a(\boldsymbol{\xi})\boldsymbol{\zeta} \tag{6.2}$$

$$\mathbf{M}(\mathbf{q})\dot{\boldsymbol{\zeta}} + \mathbf{C}(\mathbf{q}, \boldsymbol{\zeta})\boldsymbol{\zeta} + \mathbf{N}(\boldsymbol{\xi}) = \boldsymbol{\tau} \tag{6.3}$$

Where $M(q)$ is the inertia matrix, $C(q, \zeta)$ is Coriolis and centripetal matrix, $N(\zeta)$ are the potential forces and J_a is velocity transformation matrix. The velocity transformation matrix is given by

$$\mathbf{J}_a(\boldsymbol{\xi}) = \begin{bmatrix} \mathbf{R}_{0b}(\eta_2) & 0 & 0 \\ 0 & \mathbf{T}_{0b}(\eta_2) & 0 \\ 0 & 0 & \mathbf{I} \end{bmatrix} \tag{6.4}$$

where $\mathbf{I}$ denotes the identity matrix and $\mathbf{T}_{0b}$ is a matrix relating body velocities and the time derivatives of the Euler angles. Having a Jacobian matrix in the state space equation, makes it prone to singularities. Furthermore, we can also note the difference between the non-Euclidean transformation of the vehicle, where it is configuration dependent, and the Euclidean transformation of the manipulator, where is a linear and constant relation between the position and the velocity through the identity matrix.

Now that the state space is defined, the dynamics can be derived, using similar approach as previously. The velocity of link i with respect to the base frame is calculated as

$$\mathbf{V}_{0i}^{B} = \mathbf{Ad}_{T_{bi}}^{-1}\mathbf{V}_{0b}^{B} + \mathbf{V}_{bi}^{B} = \mathbf{Ad}_{T_{bi}}^{-1}\mathbf{V}_{0b}^{B} + \mathbf{Ad}_{T_{bi}}^{-1}\mathbf{J}_i\dot{\mathbf{q}} \tag{6.5}$$

where $\mathbf{V}_{0b}^{B}$ is the base velocity and $\mathbf{J}_i\dot{\mathbf{q}}$ represents the velocity of the links. In order to find the kinetic energy in terms of the link velocities represented in the link frame, we need to add the vehicle velocity represented in the base frame to the links. From here, we find that the kinematic energy of each link is given by

$$\mathcal{K} = \frac{1}{2}(\mathbf{V_{0i}^B})^{\mathbf{T}}\mathbf{I_i}\mathbf{V_{0i}^B} \tag{6.6}$$

$$=\frac{1}{2}(\mathbf{V_{0b}^B} + \mathbf{J_i}(\mathbf{q})\dot{\mathbf{q}})^{\mathbf{T}}\mathbf{Ad}_{\mathbf{T_{ib}}}^{-\mathbf{T}}\mathbf{I_i}\mathbf{Ad}_{\mathbf{T_{ib}}}^{-\mathbf{1}}(\mathbf{V_{0b}^B} + \mathbf{J_i}(\mathbf{q})\dot{\mathbf{q}}) \tag{6.7}$$

$$= \frac{1}{2}(\mathbf{V_{0b}^B} + \mathbf{J_i}(\mathbf{q})\dot{\mathbf{q}})^{\mathbf{T}}\mathbf{Ad}_{\mathbf{T_{ib}}}^{\mathbf{T}}\mathbf{I_i}\mathbf{Ad}_{\mathbf{T_{ib}}}(\mathbf{V_{0b}^B} + \mathbf{J_i}(\mathbf{q})\dot{\mathbf{q}}) \tag{6.8}$$

$$= \frac{1}{2}\Big[(\mathbf{V_{0b}^B})^{\mathbf{T}}\dot{\mathbf{q}}^{\mathbf{T}}\Big]\mathbf{M_i}(\mathbf{q})\begin{bmatrix}\mathbf{V_{0b}^B}\\ \dot{\mathbf{q}}\end{bmatrix} \tag{6.9}$$

$$= \frac{1}{2}\nu^{\mathbf{T}}\mathbf{M_i}(\mathbf{q})\nu \tag{6.10}$$

where the inertia matrix can be written in terms of the adjoint map $Ad_{T_{0i}}$ and the Jacobian j_i as

$$\mathbf{M_i}(\mathbf{q}) = \begin{bmatrix}\mathbf{Ad}_{\mathbf{T_{ib}}}^{\mathbf{T}}\mathbf{I_i}\mathbf{Ad}_{\mathbf{T_{ib}}} & \mathbf{Ad}_{\mathbf{T_{ib}}}^{\mathbf{T}}\mathbf{I_i}\mathbf{Ad}_{\mathbf{T_{ib}}}\mathbf{J_i}\\ \mathbf{J_i^T}\mathbf{Ad}_{\mathbf{T_{ib}}}^{\mathbf{T}}\mathbf{I_i}\mathbf{Ad}_{\mathbf{T_{ib}}} & \mathbf{J_i^T}\mathbf{Ad}_{\mathbf{T_{ib}}}^{\mathbf{T}}\mathbf{I_i}\mathbf{Ad}_{\mathbf{T_{ib}}}\mathbf{J_i}\end{bmatrix} \tag{6.11}$$

where $\mathbf{J_i}$ is defined as

$$\mathbf{J_i} = [\mathbf{Ad}_{\mathbf{T_{01}}}\mathbf{X_1^1} \quad \mathbf{Ad}_{\mathbf{T_{02}}}\mathbf{X_2^2} \quad \dots \quad \mathbf{Ad}_{\mathbf{T_{0i}}}\mathbf{X_i^i} \quad \mathbf{0}_{(n-i)\times 6}] \tag{6.12}$$

and $\mathbf{X_i^i}$ is the body joint twist. Given a joint i with axis p_i^i represented in $\mathscr{F}_i$, then the body joint twist is given by

$$\mathbf{X}_i^i = \begin{bmatrix}\mathbf{p}_i^i\\ \mathbf{0}\end{bmatrix} \tag{6.13}$$

Now the kinetic energy of the links are established, and with the same calculations the kinetic energy of the base, the ROV, is found by

$$\mathcal{K} = \frac{1}{2}(\mathbf{V}_{\mathbf{0i}}^{\mathbf{B}})^{\mathbf{T}}\mathbf{I_i}\mathbf{V}_{\mathbf{0i}}^{\mathbf{B}} \tag{6.14}$$

$$= \frac{1}{2}(\mathbf{H}\tilde{\mathbf{V}}_{\mathbf{0b}}^{\mathbf{B}} + \mathbf{J_i}(\mathbf{q})\dot{\mathbf{q}})^{\mathbf{T}}\mathbf{Ad}_{\mathbf{T_{ib}}}^{\mathbf{T}}\mathbf{I_i}\mathbf{Ad}_{\mathbf{T_{ib}}}(\mathbf{H}\tilde{\mathbf{V}}_{\mathbf{0b}}^{\mathbf{B}} + \mathbf{J_i}(\mathbf{q})\dot{\mathbf{q}}) \tag{6.15}$$

$$= \frac{1}{2}((\tilde{\mathbf{V}}_{\mathbf{0b}})^{\mathbf{T}}\mathbf{H}^{\mathbf{T}} + \dot{\mathbf{q}}^{\mathbf{T}}\mathbf{J_i}(\mathbf{q})^{\mathbf{T}})\mathbf{Ad}_{\mathbf{T_{ib}}}^{\mathbf{T}}\mathbf{I_i}\mathbf{Ad}_{\mathbf{T_{ib}}}(\mathbf{H}\tilde{\mathbf{V}}_{\mathbf{0b}}^{\mathbf{B}} + \mathbf{J_i}(\mathbf{q})\dot{\mathbf{q}}) \tag{6.16}$$

$$= \frac{1}{2}\left[(\tilde{\mathbf{V}}_{\mathbf{0b}}^{\mathbf{B}})^{\mathbf{T}}\dot{\mathbf{q}}^{\mathbf{T}}\right]\mathbf{M_i}(\mathbf{q})\begin{bmatrix}\tilde{\mathbf{V}}_{\mathbf{0b}}^{\mathbf{B}} \\ \dot{\mathbf{q}}\end{bmatrix} \tag{6.17}$$

$$= \frac{1}{2}\nu^{\mathbf{T}}\mathbf{M_i}(\mathbf{q})\nu \tag{6.18}$$

where $\mathbf{H}$ is a selection matrix that represents a mapping from a velocity state in $\mathbb{R}^n$ to the twist in $\mathbb{R}^6$. The inertia matrix for the rigid body, can be written as

$$\mathbf{M_b} = \begin{bmatrix}\mathbf{I_b} & \mathbf{0} \\ \mathbf{0} & \mathbf{0}\end{bmatrix} \tag{6.19}$$

Therefore, the total kinetic energy of the vehicle-manipulator system can be written as

$$\mathcal{K}(\mathbf{q}, \mathbf{V_{0b}}) = \frac{1}{2}\boldsymbol{\zeta}^{\boldsymbol{T}}\left(\sum_{\boldsymbol{i=b}}^{\boldsymbol{n}}\mathbf{M}_{\boldsymbol{i}}(\boldsymbol{q})\right)\boldsymbol{\zeta} = \frac{1}{2}\boldsymbol{\zeta}^{\boldsymbol{T}}\left(\begin{bmatrix}\mathbf{I_b} & \mathbf{0} \\ \mathbf{0} & \mathbf{0}\end{bmatrix} + \sum_{i=1}^{n}\mathbf{M}_i(\mathbf{q})\right)\boldsymbol{\zeta} \tag{6.20}$$

Since the kinetic energy is not dependent on the homogeneous transformation matrix, $\mathbf{T}_{0b}$, or the choice of inertial reference frame, the inertia matrix can be expressed in terms of the adjoint map, $\mathbf{Ad}_{T_{ib}}(q)$ and the link Jacobian $\mathbf{J}_i$ as

$$\mathbf{M}(\mathbf{q}) = \sum_{i=b}^{n}\mathbf{M_i}(\mathbf{q}) \tag{6.21}$$

$$= \sum_{i=b}^{n}(\mathbf{J}_{\mathbf{gi}}^{\mathbf{B}})^{\mathbf{T}}(\mathbf{q})\mathbf{I_i}\mathbf{J}_{\mathbf{gi}}^{\mathbf{B}}(\mathbf{q}) \tag{6.22}$$

$$= \sum_{i=b}^{n}\begin{bmatrix}\mathbf{H}^{\mathbf{T}}\mathbf{Ad}_{\mathbf{T_{ib}}}^{\mathbf{T}}\mathbf{I_i}\mathbf{Ad}_{\mathbf{T_{ib}}}\mathbf{H} & \mathbf{H}^{\mathbf{T}}\mathbf{Ad}_{\mathbf{T_{ib}}}^{\mathbf{T}}\mathbf{I_i}\mathbf{Ad}_{\mathbf{T_{ib}}}\mathbf{J_i} \\ \mathbf{J_i}^{\mathbf{T}}\mathbf{Ad}_{\mathbf{T_{ib}}}^{\mathbf{T}}\mathbf{I_i}\mathbf{Ad}_{\mathbf{T_{ib}}}\mathbf{H} & \mathbf{J_i}^{\mathbf{T}}\mathbf{Ad}_{\mathbf{T_{ib}}}^{\mathbf{T}}\mathbf{I_i}\mathbf{Ad}_{\mathbf{T_{ib}}}\mathbf{J_i}\end{bmatrix} \tag{6.23}$$

where $\mathbf{J}_{\mathbf{gi}}^{\mathbf{B}} = [\mathbf{Ad}_{\mathbf{T_{ib}}}\mathbf{H} \;\; \mathbf{Ad}_{\mathbf{T_{ib}}}\mathbf{J_i}]$. Furthermore, the dynamics follows form the Lagrangian equation, where the potential forces $\mathcal{U}$, also are included

$$\sum_{i=b}^{n}\left\{(\mathbf{J}_{gi}^{B})^{T}\left[\frac{d}{dt}\frac{\partial\mathcal{K}_i}{\partial\mathbf{V}_{0i}^{B}}+\begin{bmatrix}\hat{\boldsymbol{\omega}}_{0i}^{B} & \mathbf{0}\\ \hat{\boldsymbol{\nu}}_{0i}^{B} & \hat{\boldsymbol{\omega}}_{0i}^{B}\end{bmatrix}\frac{\partial\mathcal{K}_i}{\partial\mathbf{V}_{0i}^{B}}+\frac{\partial\mathcal{U}}{\partial\boldsymbol{\eta}_{0i}}\right]\right\}=\boldsymbol{\tau}$$

$$\sum_{i=b}^{n}[(\mathbf{J}_{gi}^{B})\mathbf{I}_i\mathbf{J}_{gi}^{B}]\dot{\boldsymbol{\zeta}}+\sum_{i=b}^{n}[\mathbf{J}_{gi}^{B})\mathbf{I}_i\dot{\mathbf{J}}_{gi}^{B}-(\mathbf{J}_{gi}^{B})^{T}\mathbf{W}_i\mathbf{J}_{gi}^{B}]\boldsymbol{\zeta}+(\mathbf{J}_{gi}^{B})^{T}\frac{\partial\mathcal{U}}{\partial\boldsymbol{\eta}_{0i}}=\boldsymbol{\tau} \tag{6.24}$$

Thus, we can get the dynamics on the desired matrix form, as shown in (6.25) and (6.26)

$$\dot{\boldsymbol{\xi}}=\mathbf{J}_a(\boldsymbol{\xi})\boldsymbol{\zeta} \tag{6.25}$$

$$\mathbf{M}(\mathbf{q})\dot{\boldsymbol{\zeta}}+\mathbf{C}(\mathbf{q},\boldsymbol{\zeta})\boldsymbol{\zeta}+\mathbf{N}(\boldsymbol{\zeta})=\boldsymbol{\tau}. \tag{6.26}$$

The inertia matrix is given by

$$\mathbf{M}(\mathbf{q})=\sum_{i=b}^{n}(\mathbf{J}_{\mathbf{gi}}^{\mathbf{B}})^{\mathbf{T}}(\mathbf{q})\mathbf{I_i}\mathbf{J}_{\mathbf{gi}}^{\mathbf{B}}(\mathbf{q}) \tag{6.27}$$

The Coriolis matrix is given by

$$\sum_{i=b}^{n}(\mathbf{J}_{\mathbf{gi}}^{\mathbf{B}})^{\mathbf{T}}(\mathbf{q})\mathbf{I_i}\dot{\mathbf{J}}_{\mathbf{gi}}^{\mathbf{B}}(\mathbf{q})-(\mathbf{J}_{\mathbf{gi}}^{\mathbf{B}})^{\mathbf{T}}(\mathbf{q})\mathbf{W_i}(\mathbf{V}_{\mathbf{0i}}^{\mathbf{B}})\mathbf{J}_{\mathbf{gi}}^{\mathbf{B}}(\mathbf{q}) \tag{6.28}$$

where

$$\mathbf{W_i}(\mathbf{V}_{\mathbf{0i}}^{\mathbf{B}})=\begin{bmatrix}\mathbf{0} & \frac{\partial\hat{\mathcal{K}}_{\mathbf{i}}}{\partial\nu_{\mathbf{0i}}^{\mathbf{B}}}\\ \frac{\partial\hat{\mathcal{K}}_{\mathbf{i}}}{\partial\nu_{\mathbf{0i}}^{\mathbf{B}}} & \frac{\partial\hat{\mathcal{K}}_{\mathbf{i}}}{\partial\omega_{\mathbf{0i}}^{\mathbf{B}}}\end{bmatrix} \tag{6.29}$$

and the potential forces are given as

$$\mathbf{N}(\boldsymbol{\xi})=\sum_{i=b}^{n}(\mathbf{J}_{\mathbf{gi}}^{\mathbf{B}})^{\mathbf{T}}(\mathbf{q})\mathbf{Ad}_{\mathbf{T_{0b}(T_{i0}}},\mathbf{q})\mathbf{F}_{\mathbf{g}}^{\mathbf{i}}(\mathbf{T_{0b}},\mathbf{q}) \tag{6.30}$$

where $\mathbf{F}_{\mathbf{g}}^{\mathbf{i}}$ are the potential forces of link i in the manipulator.(From 2014) (Eidsvik 2018)

The derivation of $\mathbf{J}_{gi}^{B}$ and $\mathbf{W}_i$ can be seen the Appendix.

Chapter 7

Method

This chapter concerns the method used to simulate the system. For this master thesis, *MATLAB* and *Simulink* was the two software's used for modelling and simulation. *MATLAB* was mainly used to perform the necessary calculations regarding the different matrices, while *Simulink* were used to build the UVMS model and simulate the dynamics and the response of the system. All the mathematical calculations are based on the theory presented in the previous chapters.

7.1 UVMS Model

The following section will present the *Simulink*-model used to simulate the system, and all the relevant blocks will be reviewed. The *Simulink*-model for the underwater vehicle-manipulator system is presented in Figure 7.1.

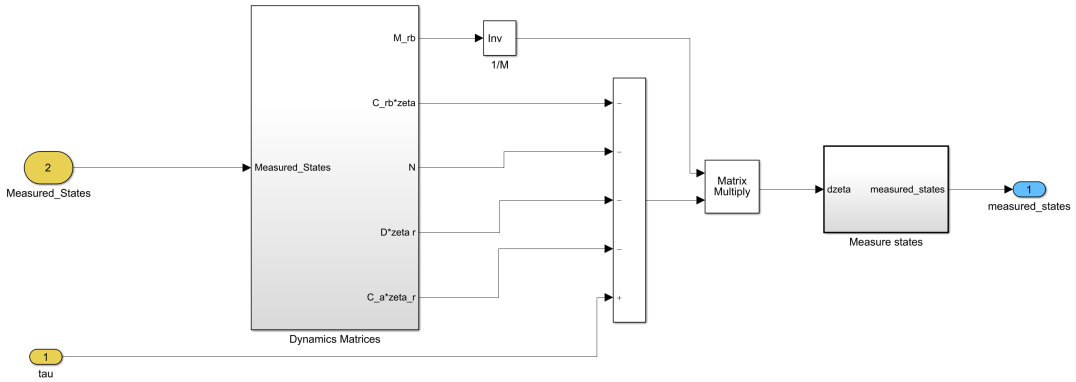

Figure 7.1: Underwater vehicle-manipulator system modelled in *Simulink*

This overview shows the dynamics of the simulation. The different matrices used to model the EOM is calculated in the block called "Dynamic Matrices". These are added together before multiplied with the inverse of the mass matrix to create the second order derivative term in the EOM, and then used as an input to the "Measure states" block. The system has two different input signals and only one output, where the "measured_states" is the feedback-term. "measured_states is a *MATLAB*-structure containing the different states, transformation matrices and jacobians, needed to perform the calculations of the dynamic matrices.

7.1.1 Dynamic Matrices

The modelling and calculation of the matrices is shown in Figure 7.2.

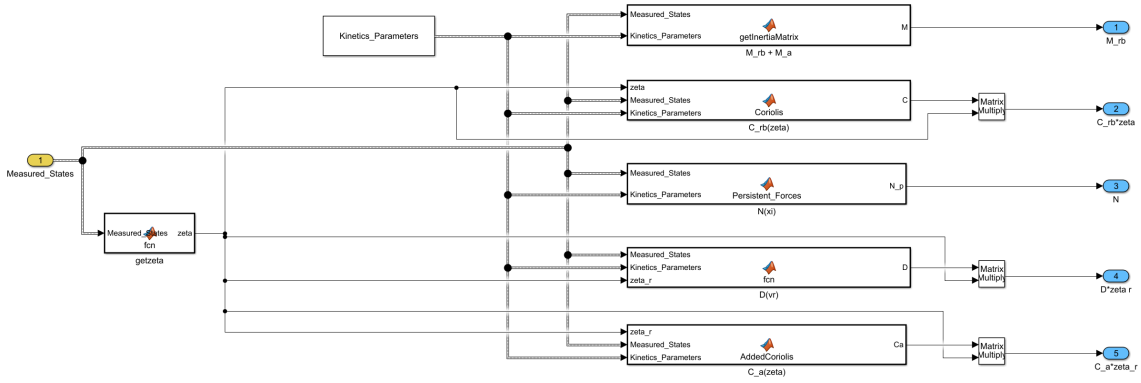

Figure 7.2: Calculation of dynamic matrices

Each of the matrices are calculated in separate *MATLAB*-scripts, before three of them are multiplied with the ζ-vector and given as output, as seen from Figure 7.1. The input to this block is the "Measured_States"-term and the "getzeta" function retrieves the velocities of the system, which is used as input to several matrix-calculations. Constants and other physical properties are defined and given as input to the model.

7.1.2 Measure States

The "Measure states"-block, from Figure 7.1, is presented in Figure 7.3.

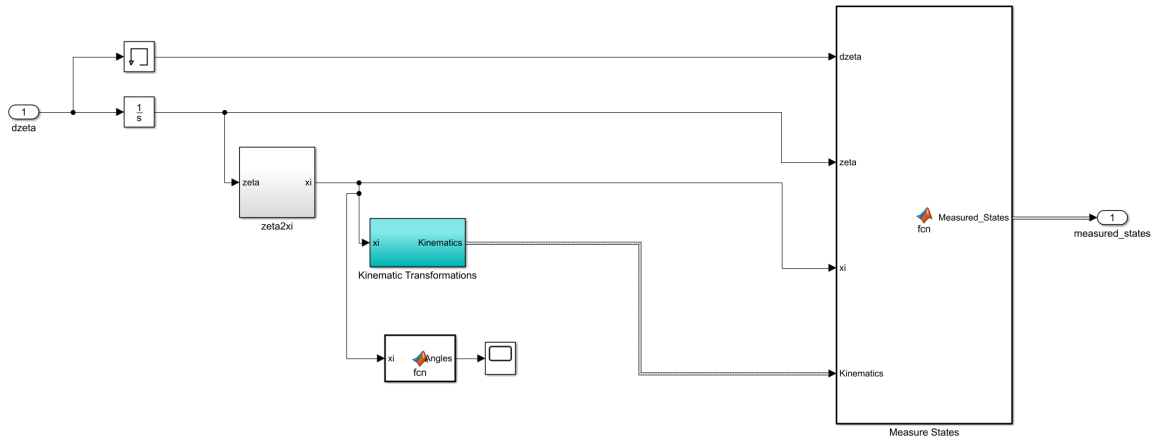

Figure 7.3: Calculation of dynamic matrices

In this block, the "Measure_states"-term is created. This is the input and output of the UVMS-model, and contains all the information of the system, i.e. the accelerations, velocities and position of the system, and transformation matrices and Jacobians, as stated before. The acceleration is directly given from the derivative of ζ, while the velocities are calculated by integration. When ζ is calculated, it is both stored in the "Measure_states"-term and used to calculate the position and orientation of the system, which is performed in the "zeta2xi"-block. "xi" is a vector containing the position and orientation of the ROV, as well as the joint angles of the manipulator. This state-vector is also stored in the "Measure_states" structure.

7.1.2.1 zeta2xi

Figure 7.4 shows the model which is calculating the position and orientation of the ROV, and the joint angles of the manipulator.

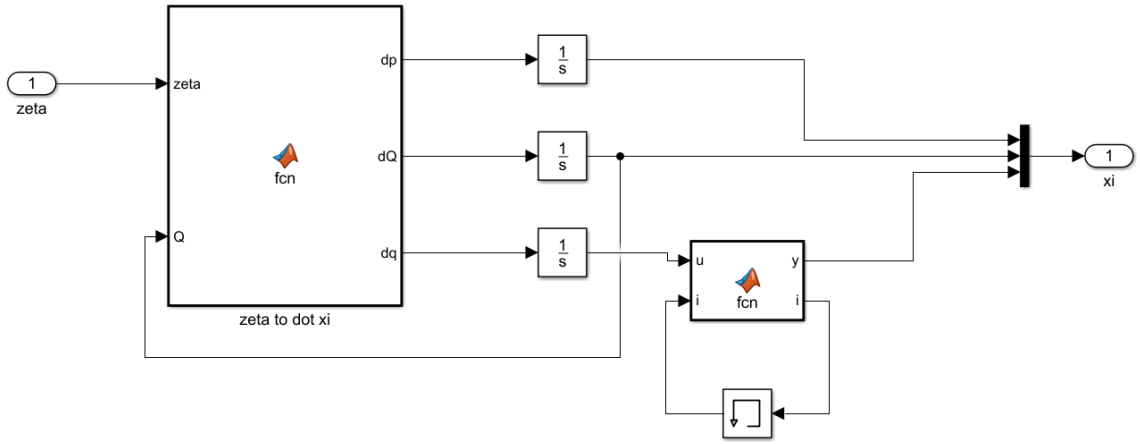

Figure 7.4: Calculation of dynamic matrices

The orientation comes with a quaternion representation, which is implemented in the *MATLAB*-script called "zeta to dot xi". The output of this script is the derivative of the position, orientation and the joint angles, which further on is integrated before they are given as an output. The second *MATLAB*-script contains a simple algorithm to add rotation to the manipulator joints. This is done by adding a constant angular velocity to the joint different joints.

7.1.2.2 Kinematic Transformations

The kinematic transformation subsystem, shown in Figure 7.5, calculates the different transformation matrices and jacobians needed to calculate the dynamic matrices. The manipulator's' configuration is updated here, which is later on used to calculate the different dynamic properties for that certain configuration. This information is an output in the form of a structure, which is stored in the "Measure_states"-term.

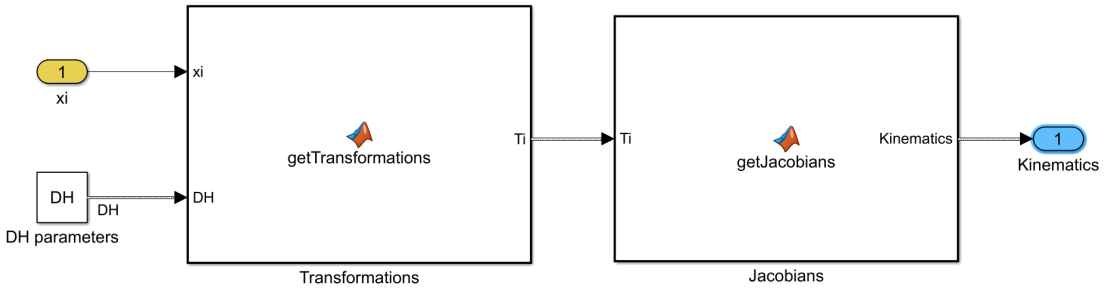

Figure 7.5: Calculation of dynamic matrices

7.2 Numerical Values of the Matrices Used in the Simulations

Some of the matrices used in the simulations regarding the ROV are constant. This means that they are predefined and not needed to be calculated for every iteration as the other matrices. All the manipulator matrices are calculated in-loop, while the mass matrices and damping matrices for the ROV are pre-defined. The numerical values of these matrices are given below.

$$M_{RB} = \begin{bmatrix} 1700 & 0 & 0 & 0 & 0 & 0 \\ 0 & 1700 & 0 & 0 & 0 & 0 \\ 0 & 0 & 1700 & 0 & 0 & 0 \\ 0 & 0 & 0 & 1381.6 & 0 & 0 \\ 0 & 0 & 0 & 0 & 1314.60 & \\ 0 & 0 & 0 & 0 & 0 & 704 \end{bmatrix} \tag{7.1}$$

$$M_A = \begin{bmatrix} 550.9 & 0 & -70 & 0 & -28 & 0 \\ 0 & 995.3 & 0 & -185 & 0 & -18 \\ -70 & 0 & 7311 & 0 & 105 & 0 \\ 0 & -185 & 0 & 977.6 & 0 & -41 \\ -28 & 0 & 105 & 0 & 2244 & 0 \\ 0 & -18 & 0 & -41 & 0 & 491.9 \end{bmatrix} \tag{7.2}$$

$$D_L = \begin{bmatrix} 55.9736 & 0 & 0 & 0 & 0 & 0 \\ 0 & 61.6000 & 0 & 0 & 0 & 0 \\ 0 & 0 & 631.5183 & 0 & 0 & 0 \\ 0 & 0 & 0 & 132.9311 & 0 & 0 \\ 0 & 0 & 0 & 0 & 456.4635 & 0 \\ 0 & 0 & 0 & 0 & 0 & 100.8714 \end{bmatrix} \tag{7.3}$$

$$D_Q = \begin{bmatrix} 561.7 & 0 & 0 & 0 & 0 & 0 \\ 0 & 878.7 & 0 & 0 & 0 & 0 \\ 0 & 0 & 1578.8 & 0 & 0 & 0 \\ 0 & 0 & 0 & 330.4 & 0 & 0 \\ 0 & 0 & 0 & 0 & 1143.1 & 0 \\ 0 & 0 & 0 & 0 & 0 & 363.4 \end{bmatrix} \tag{7.4}$$

Chapter 8

Results

In this section the result of the simulations are presented. The main goal of the simulations is to observe the response of the ROV when the manipulator either are standing still in different configurations, or performing simple movements. For the simulations three different manipulator configurations are considered. Firstly, the manipulator is configured in a stowed position, secondly, it is fully extended in x-direction, and lastly, the manipulator is fully extended in negative z-direction. The simulations with the manipulator in stowed position are performed with intentions to cover the vehicle-manipulator interaction when the manipulator is idle. As for the other two configurations, they are chosen too represent commonly used configurations while the UVMS is in operation, as well as obtain the greatest magnitudes regarding the response. It is not necessary simulate a whole lot of configuration between the stow-configuration and the maximum reach configuration, this is mainly because the response will be of the same sort, just with a decreased response magnitude.

8.1 Manipulator in Stowed Position

In the first simulation the manipulator has its stowed configuration. The joint angles are constant though out the simulation, where all of them are set to zero except for the wrist pitch angle, which is set to -90° to straighten out the arm.

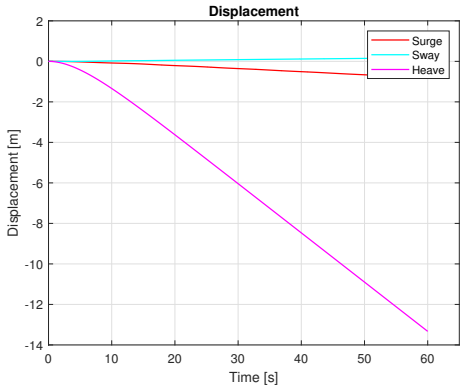

(a) Displacement of the ROV

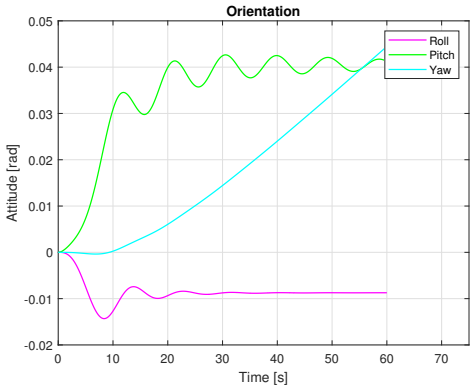

(b) Orientation of the ROV

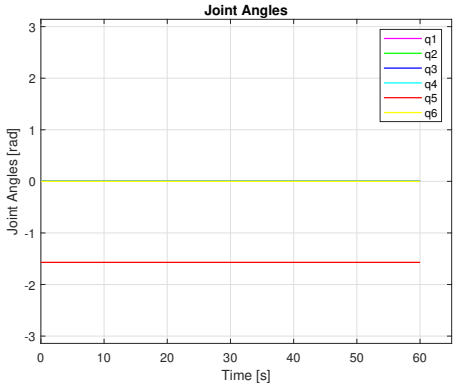

(c) Manipulator joint angles

Figure 8.1: Response of the system to a stowed manipulator

The displacement of the ROV in Figure 8.1a shows small response amplitudes in surge and sway, but a quite significant response in heave. As for the orientation, presented in Figure 8.1b, the rotations are only around $-0.001 - 0.04\,[rad]$, which is around $0.5° - 2.3°$. The simulation duration was set to 60 seconds, as this was an appropriate time interval to determine the response. At the end of each simulation all the oscillations are dying out, and the heave and yaw response is continuing in the same order.

8.2 Manipulator Fully Extended

In the second simulation case, the manipulator is at its maximum reach in the x-direction, or straight forward seen form the ROV. There are performed two different simulations for this case, one for when the manipulator is still and one for when it starts at its maximum reach configuration and ends at the stow configuration.

8.2.1 Standing Still

The following joint angles were used in this simulation:

$$\mathbf{q} = [0^\circ \ -60^\circ \ 120^\circ \ 0^\circ \ -60^\circ \ 0^\circ] \tag{8.1}$$

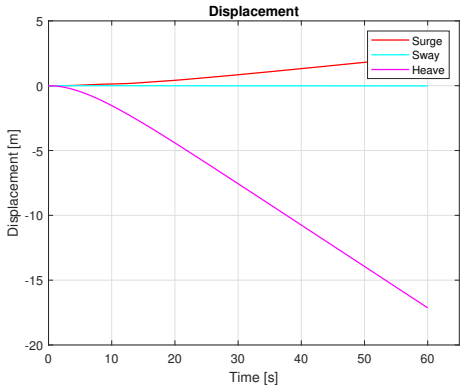

(a) Displacement of the ROV

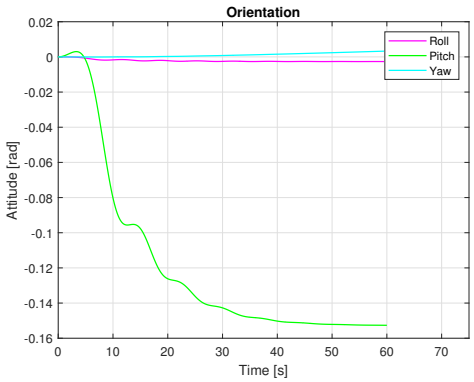

(b) Orientation of the ROV

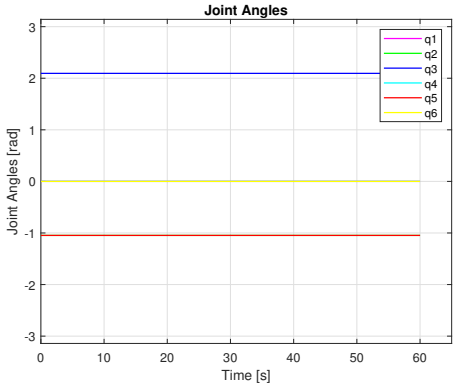

(c) Manipulator joint angles

Figure 8.2: Response when the manipulator is at its full reach

8.2.2 Moving

To simulate a movement of the fully extended manipulator, the base yaw was linearly increased from 0° to 60°. Since the manipulator has a 120° limitation of the base yaw, which is 60° to each side from the stow position, a simulation where the manipulator is moving in the area of $0^\circ - 60^\circ$ is chosen. The following start and end configuration were used

$$\mathbf{q_{start}} = [0^\circ \ -60^\circ \ 120^\circ \ 0^\circ \ -60^\circ \ 0^\circ]^T \tag{8.2}$$

$$\mathbf{q_{end}} = [60^\circ \ -60^\circ \ 120^\circ \ 0^\circ \ -90^\circ \ 0^\circ]^T \tag{8.3}$$

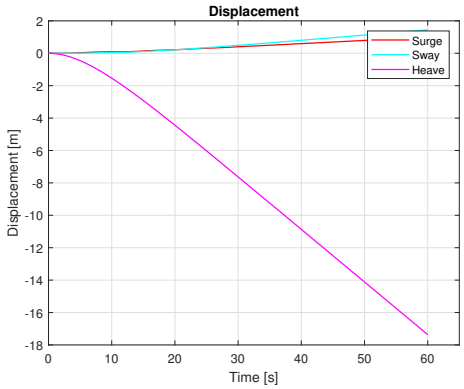

(a) Displacement of the ROV

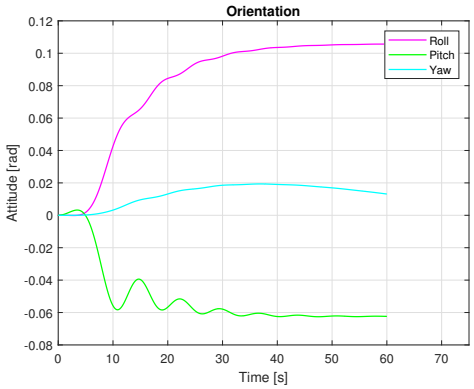

(b) Orientation of the ROV

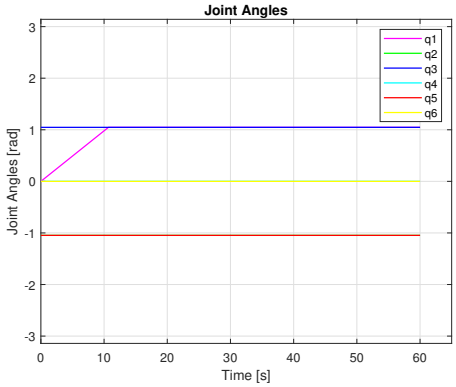

(c) Manipulator joint angles

Figure 8.3: Response when the manipulator is fully extended and moving

Figure 8.3c shows the joint angle representing the base yaw of the manipulator is changing to simulate a fully extended manipulator rotating to the left, as seen from the ROV. The displacement is shown in Figure 8.3a, while the orientation is shown in Figure 8.3b.

8.3 Manipulator Oriented Downwards

For the last simulation the manipulator is configured to its max reach in the negative z-direction. This configuration is supposed to represent the configuration when the manipulator is picking something up from the ground beneath the ROV.

8.3.1 Standing Still

For when the manipulator is standing still the following joint angles were used

$$\mathbf{q} = [0^\circ \ -60^\circ \ 60^\circ \ 0^\circ \ -90^\circ \ 0^\circ]^T \tag{8.4}$$

Figure 8.4 shows the total response of the UVMS.

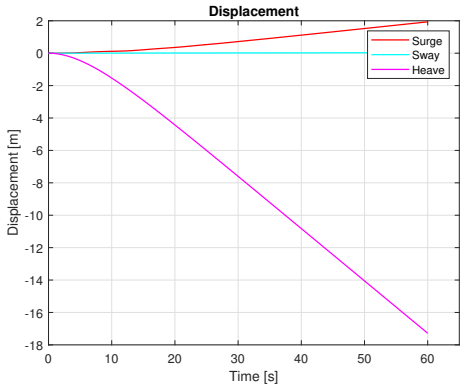

(a) Displacement of the ROV

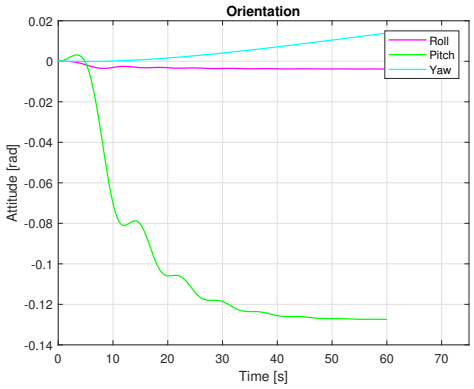

(b) Orientation of the ROV

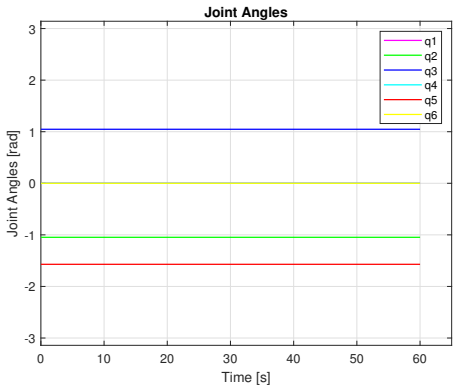

(c) Manipulator joint angles

Figure 8.4: Response when the manipulator is standing still and oriented downwards

8.3.2 Moving

To simulate a relevant scenario where the manipulator is moving, the manipulator starts being oriented in the negative z-direction and moves towards the stow position. This represents the movement from when the manipulator is picking objects up from the ground and transports it back to the ROV. The following start and stop configurations were used

$$\mathbf{q_{start}} = [0^\circ \ -60^\circ \ 60^\circ \ 0^\circ \ -90^\circ \ 0^\circ]^T \tag{8.5}$$

$$\mathbf{q_{end}} = [0^\circ \ 0^\circ \ 0^\circ \ 0^\circ \ -90^\circ \ 0^\circ]^T \tag{8.6}$$

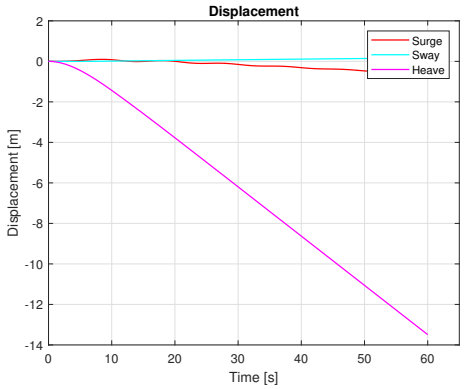

(a) Displacement of the ROV

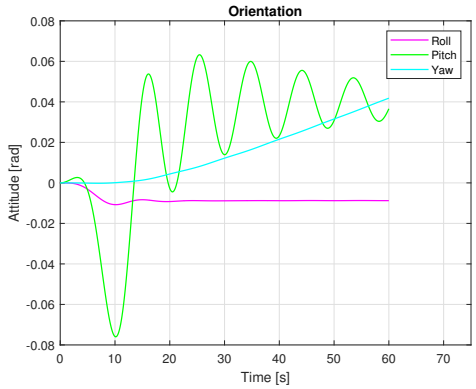

(b) Orientation of the ROV

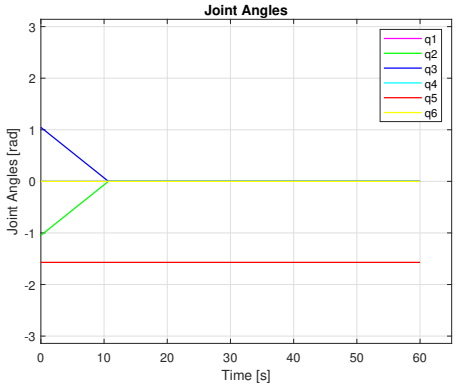

(c) Manipulator joint angles

Figure 8.5: Response when the manipulator is configured downwards

Figure 8.5c shows the rotation of the manipulators' shoulder and elbow pitch. The total rotation is 60° over a period of ten seconds. The displacement and orientation is showed in Figure 8.5a and 8.5b. Compared to the previous simulations, the pitch oscillations is of greater significance. It oscillates between $[-0.08,\ 0.06]$ $[rad]$ to begin with, before it stabilizes around 0.04 $[rad]$.

Chapter 9

Discussion

This chapter has the intention to analyze and discuss the results in section 8 in the same order as they were presented.

9.1 Manipulator in Stowed Position

This section mainly concerns Figure 8.1. These plots presents the results of the simulations performed when the manipulator is at its stowed position. There are no manipulator movements present, hence the joint angles are constant for the whole duration of the simulation.

Figure 8.1a, shows small displacements in surge and sway, while heave is significantly larger. On its own, the ROV is a neutrally or slightly positive buoyant system. However, the extra weight of the manipulator makes the gravitational force on the system larger than the buoyancy, making the system to sink, instead of staying neutrally or positive buoyant. Since the ROV has no restoring force in the translation DOF's there is nothing that is gonna prevent the system from sinking as a results of the added system mass, hence the heave response as observed in Figure 8.1a. The surge and sway response is of insignificant magnitudes, and does not lead to any notable response. Since the manipulator mainly affects the ROV in the z-direction, because of the gravitational force, the response in x- and y-direction will obviously be small. Nevertheless, coupling forces and displacements creates forces in several dimensions, which results in the small responses in other DOFs.

Since the manipulator is mounted in front of the ROV, the forces created which affects the ROV will therefore result in mainly moments about the local y-axis. These moments will make the ROV rotate around the y-axis, also called pitching. The form of the roll and pitch motion, as seen in Figure 1.4a, is characterized by it oscillatory motion. This motion is a result of the restoring forces present in these DOF's. On the contrary, the yaw motion is a more linear motion, because there are no forces counter acting

any rotations around the local z-axis. The magnitude of the pitch motion, which is the most dominant motion amongst the rotational motions, is about 0.04 [rad] which is approximately 2.3°. This is not a significantly large rotation, but it indicates that the system needs actuation in order to stabilize, as it is not capable of doing it on its own. This is also in a static position, where dynamic forces are negligible, so greater responses will occur when dynamic motion are included.

9.2 Manipulator Fully Extended

For the simulations when the manipulator is is at its maximum reach straight ahead of the ROV, two different cases were simulated. One where the manipulator is standing still, and one where it rotates 60° to the left side of the ROV.

As seen from Figure 8.2 and 8.3, the displacement of the system is relatively similar. The surge and sway response is quite insignificant, while the heave motion, as with the first simulation, steadily decreases throughout the simulation.

On the other hand, the differences between the rotations are more notable. When the manipulator is standing still, the pitch motion is the only rotation of significance. Since the are no movement involved, there are little coupling effects, and therefore responses mainly in one DOF. The magnitude of the pitch motion when the manipulator is fully extended is quite larger then when stowed. When fully extended the pitch motion can reach a rotation of about 8.6°. This enlargement of the rotation comes from the configuration of the manipulator. When it is fully extended, the distance from the manipulator base to the end-effector has increased, meaning that the moment arm is larger, which results in larger moments about the local y-axis. When moments increase, the rotation also increases, as seen from the simulations. When the manipulator rotates 60° to left, other rotational motions becomes significant. The movement of the manipulator creates forces in other directions, and moments about the x-axis and z-axis occur. As seen from Figure 8.3b, the roll motion is greater than the yaw motion. This is mainly a result of the forces created when manipulator rotates. When it rotates to the left, a moment arm to the x-axis arises, and increases proportionally as the base of the manipulator rotates. When it has rotated 60°, the moment arm is at its maximum, and the gravitational forces creates moments about the x-axis, causing this roll motion. As for the yaw motion, since the movement of the manipulator mainly is in the xy-plane, the gravitational forces does not create any moments about the z-axis, so the yaw motion will be of lesser magnitude. However, the moments created about the x- and y-axis, makes the ROV tilt to either of the sides, and this tilt contributes to small force components that creates moments about the z-axis. These forces and moments creates the small yaw motion.

9.3 Manipulator Oriented Downwards

In the last simulation case, the manipulator was oriented downwards, to represent the position of the manipulator when it is picking objects up from the ground. It is performed two different simulations with this configuration, one where the manipulator is fixed in this position, and one where it moves back to the stowed position. The results from these simulations is showed in Figure 8.4 and 8.5. The displacement of the system for this configuration is very similar to the other simulations, where the surge and sway is of small magnitudes and the heave motion is strictly decreasing throughout the simulation.

Figure 8.5c shows the rotation of joint $q2$ and $q3$ to obtain the desired motion. The starting point is $\pm 60°$, respectively, and both ends at $0°$ after approximately 10 seconds. Similarly as the previous simulation including motion of the manipulator, the rotational speed is constant.

The rotational response of the system can be seen in Figure 8.4b and 8.5. Clearly, the pitch motion is the dominant rotation. Since the manipulator is oriented downwards, the largest force components created will be along the z-axis, and the largest moments created is about the y-axis. However, there exist small moment contribution in the other dimensions as well, leading to the observed roll and yaw motion. The large pitch oscillations seen in Figure 8.5b, comes from the forces created by the manipulator motion and the restoring forces of the ROV trying to counter act the moments created. Amplitude wise, the oscillations experienced in this simulation, is the largest of all the simulations performed. This comes as a results of the motion mainly being directed along one axis, mainly the z-axis, so the moments created are focused around one specific axis, making it harder for the restoring forces to counter act the motion.

Chapter 10

Conclusion

In this master thesis an underwater vehicle-manipulator system was modelled. The UVMS consisted of the ROV Minerva 2, and the manipulator Orion 7R. The purpose was to calculate and simulate the interaction between the manipulator and the ROV, and to see how the ROV would respond to different manipulator configurations and simple movements.

To model the UVMS, a second order differential equation, the equation of motion, was used. This is a common equation used to describe surface vessel and underwater vehicles, including vehicle-manipulator systems. After the necessary matrices were obtained, the equation was transformed into Laplace-domain and modelled in Simulink, which was used for simulations.

The simulation covered three different manipulator configurations, stowed position, fully extended in x-direction and fully extended in negative z-direction. For the two fully extended simulations, some movements of the manipulator was included, where some of the joints were rotating during the simulation. This had the purpose of cover basic movements of the manipulator, and to observe how Minerva 2 responded to these movements.

The results showed that Minerva 2 mainly experienced pitch and roll motion, and the restoring forces were able to counter act these rotations, and stabilize the system at a couple of degrees of rotation. Since roll and pitch are the only DOFs with restoring forces, the responses in the other 4 DOFs could not counter act the applied forces, and therefore continued to increase during the simulation when there was forces present in the certain DOFs.

10.1 Further Work

Now that a model for the UVMS consisting of Minerva 2 and Orion 7R is built, control systems, for both the ROV and the manipulator, should be added. So far, the model

can simulate the response the ROV experiences from manipulator configurations and movements. Now, the ROV needs to counter act these displacements and rotations, in order to keep the system stable. Since Minerva 2 is sufficiently actuated, designing a controller to counter act forces and moments in all the DOFs is possible.

In addition to a controller for the ROV, an controller for the manipulator is also necessary. In this master thesis all the movement and rotations of the manipulator joints are done by adding a constant angular velocity to joints. This, however, is preferably done by a controller that calculates a path for the joints to follow, and how to follow it.

Sine the manipulator is mounted on the ROV to perform intervention tasks, it is needed to model the contact forces between the manipulator and the surroundings, and how these forces will affect the ROV. The ROV needs to keep stable while the manipulator performs its tasks, and it is therefore vital that these interactions are accurately modelled.

Appendices

Appendix A

Differentiation of Jacobian Matrix

Following, the differentiation of the Jacobian matrix used to calculate the Coriolis matrix is derived.

$$\dot{\mathbf{J}}_{gi}^{B} = \frac{d}{dt}\left(\begin{bmatrix}\mathbf{Ad}_{gbi}^{-1} & \mathbf{Ad}_{gbi}^{-1}\mathbf{J}_i\end{bmatrix}\right) \tag{A.1}$$

$$= \begin{bmatrix}\frac{d}{dt}\mathbf{Ad}_{gbi}^{-1} & \frac{d}{dt}(\mathbf{Ad}_{gbi}^{-1})\mathbf{J}_i + \mathbf{Ad}_{gbi}^{-1}\frac{d}{dt}(\mathbf{J}_i)\end{bmatrix} \tag{A.2}$$

where

$$\frac{d}{dt}\mathbf{Ad}_{gbi}^{-1} = \frac{d}{dt}\begin{bmatrix}\mathbf{R}_{bi}^{T} & -\mathbf{R}_{bi}^{T}\widehat{\mathbf{p}}_{bi} \\ 0 & \mathbf{R}_{bi}^{T}\end{bmatrix} \tag{A.3}$$

$$= \begin{bmatrix}\mathbf{R}_{bi}^{T}\widehat{\omega}_{ib}^{b} & -\mathbf{R}_{bi}^{T}\widehat{\omega}_{ib}^{b}\widehat{\mathbf{p}}_{bi} + \mathbf{R}_{bi}^{T}\dot{\widehat{\mathbf{p}}}_{bi} \\ 0 & \mathbf{R}_{bi}^{T}\widehat{\omega}_{ib}^{b}\end{bmatrix} \tag{A.4}$$

$$\tag{A.5}$$

where the following properties are used

$$\dot{\mathbf{R}}_{ab} = \mathbf{R}_{ab}\widehat{\omega}_{ab}^{b} \tag{A.6}$$

$$\mathbf{R}_{bi} = (\mathbf{R}_{ib})^{T} \tag{A.7}$$

and where

$$\boldsymbol{\omega}_{bk}^{k} = \boldsymbol{\omega}_{0k}^{k} - (\mathbf{R}_{bk})^{T}\boldsymbol{\omega}_{0b}^{b} \tag{A.8}$$

Now we get that

$$\boldsymbol{\omega}_{ib}^{b} = \boldsymbol{\omega}_{0b}^{b} - \mathbf{R}_{bi}\begin{bmatrix}\mathbf{0}_{3\times3} & \mathbf{I}_{3\times3}\end{bmatrix}\left(\mathbf{J}_{gi}^{B}\boldsymbol{\zeta}\right) \tag{A.9}$$

The time derivative of $\mathbf{p}_{bi}$ is

$$\dot{\mathbf{p}}_{bi} = \mathbf{R}_{bi}\mathbf{H}\mathbf{A}\mathbf{d}_{gbi}^{-1}\mathbf{J}_{i}\dot{\mathbf{q}} \tag{A.10}$$

where

$$\mathbf{H} = \begin{bmatrix}\mathbf{I}_{3\times3} & \mathbf{0}_{3\times3}\end{bmatrix} \tag{A.11}$$

Appendix **B**

Derivation of $\mathbf{W}_i$

The matrix $\mathbf{W}_i$, used to calculate the Coriolis matrix is derived below.

$$\mathbf{W_i}(\mathbf{V_{0i}^B}) = \begin{bmatrix} \mathbf{0} & \frac{\partial \hat{\mathcal{K}}_\mathbf{i}}{\partial v_{\mathbf{0i}}^\mathbf{B}} \\ \frac{\partial \hat{\mathcal{K}}_\mathbf{i}}{\partial v_{\mathbf{0i}}^\mathbf{B}} & \frac{\partial \hat{\mathcal{K}}_\mathbf{i}}{\partial \omega_{\mathbf{0i}}^\mathbf{B}} \end{bmatrix} \tag{B.1}$$

$$\mathcal{K}_i = \frac{1}{2}(\mathbf{V}_{0i}^B)^T \mathbf{I}_i \mathbf{V}_{0i}^B \tag{B.2}$$

$$= \frac{1}{2}\begin{bmatrix} (\boldsymbol{v}_{0i}^B)^T & (\boldsymbol{\omega}_{0i}^B)^T \end{bmatrix} \begin{bmatrix} m\mathbf{I}_{3\times 3} & -m\widehat{\mathbf{r}}_g^b \\ m\widehat{\mathbf{r}}_g^b & \mathbf{I}_b \end{bmatrix} \begin{bmatrix} \boldsymbol{v}_{0i} \\ \boldsymbol{\omega}_{0i}^B \end{bmatrix} \tag{B.3}$$

$$= \frac{1}{2}\left(m(\boldsymbol{v}_{0i}^B)^T \mathbf{I}_{3\times 3} \boldsymbol{v}_{0i}^B + m(\boldsymbol{\omega}_{0i}^B)^T \widehat{\mathbf{r}}_g^b \boldsymbol{v}_{0i}^B - m(\boldsymbol{v}_{0i}^B)^T \widehat{\mathbf{r}}_g^b \boldsymbol{\omega}_{0i}^B + (\boldsymbol{\omega}_{0i}^B)^T \mathbf{I}_b \boldsymbol{\omega}_{0i}^B \right) \tag{B.4}$$

$$= \frac{1}{2}\left(m(\boldsymbol{v}_{0i}^B)^T \mathbf{I}_{3\times 3} \boldsymbol{v}_{0i}^B + 2m(\boldsymbol{v}_{0i}^B)^T \widehat{\mathbf{r}}_g^b \boldsymbol{\omega}_{0i}^B + (\boldsymbol{\omega}_{0i}^B)^T \mathbf{I}_b \boldsymbol{\omega}_{0i}^B \right) \tag{B.5}$$

$$= \frac{1}{2}\left(m(\boldsymbol{v}_{0i}^B)^T \mathbf{I}_{3\times 3} \boldsymbol{v}_{0i}^B + 2m(\boldsymbol{\omega}_{0i}^B)^T \widehat{\mathbf{r}}_g^b \boldsymbol{v}_{0i}^B + (\boldsymbol{\omega}_{0i}^B)^T \mathbf{I}_b \boldsymbol{\omega}_{0i}^B \right) \tag{B.6}$$

$$\frac{\partial \mathcal{K}_\mathbf{i}}{\partial v_{\mathbf{0i}}^\mathbf{B}} = m\mathbf{I}_{3\times 3}\boldsymbol{v}_{0i}^B - m\widehat{\mathbf{r}}_g^b \boldsymbol{\omega}_{0i}^B \tag{B.7}$$

$$\frac{\partial \hat{\mathcal{K}}_\mathbf{i}}{\partial \omega_{\mathbf{0i}}^\mathbf{B}} = \mathbf{I}_b \boldsymbol{\omega}_{0i}^B + m\widehat{\mathbf{r}}_g^b \boldsymbol{v}_{0i}^B \tag{B.8}$$

where $\mathbf{I}_b$is the inertia matrix and $\mathbf{r}_g^b$ is the vector from the origin of link i to centre of gravity of link i.

Bibliography

[1] John J Craig. *Introduction to robotics : mechanics and control*. eng. Reading, Mass, 1989.

[2] Fredrik Dukan. *Thesis on ROV Motion Control Systems*. NTNU, 2014.

[3] Ole A. N. Eidsvik. *Dynamics of remotely operated underwater vehicle systems*. eng. Trondheim, 2018.

[4] Thor I. Fossen. *Handbook of Marine Craft Hydrodynamics and Motion Control*. John Wiley & Sons, 2011.

[5] Pål Johan From. *Vehicle-Manipulator Systems : Modeling for Simulation, Analysis, and Control*. eng. London, 2014.

[6] Westwood Global Energy Group. "World ROV Operations Market Forecast 2018-2022". In: (2018).

[7] Erik Bjørklund Holven. *Control System for ROV Minerva 2*. eng. 2018. URL: http://hdl.handle.net/11250/2564521.

[8] Hai Huang et al. "Vehicle-manipulator system dynamic modeling and control for underwater autonomous manipulation". eng. In: *Multibody System Dynamics* 41.2 (2017), pp. 125–147. ISSN: 1384-5640.

[9] T Mclain, S Rock, and Mj Lee. "Experiments in the coordination of underwater manipulator and vehicle control". eng. In: *MTS/IEEE, NEW YORK, NY (USA). Vol. 2, pp. 1208-1215. 1995.* Vol. 2. McLain, McLain. 1995, pp. 1208–1215. ISBN: 0933957149. URL: http://search.proquest.com/docview/15586774/?pq-origsite=primo.

[10] S. Mcmillan, D.E. Orin, and R.B. Mcghee. "Efficient dynamic simulation of an underwater vehicle with a robotic manipulator". eng. In: *Systems, Man and Cybernetics, IEEE Transactions on* 25.8 (1995), pp. 1194–1206. ISSN: 0018-9472.

[11] Richard M Murray. *A mathematical introduction to robotic manipulation*. eng. Boca Raton, Fla, 1994.

[12] FMC Technologies Schilling Robotics. "Schilling Robotics ORION 7P and 7R". In: (2013).

[13] Jee-Hwan Ryu, Dong-Soo Kwon, and Pan-Mook Lee. "Control of underwater manipulators mounted on an ROV using base force information". eng. In: vol. 4. USA: IEEE, 2001, pp. 3238–3243. ISBN: 0780365763.

[14] N. Sarkar and T.K. Podder. “Coordinated motion planning and control of autonomous underwater vehicle-manipulator systems subject to drag optimization”. eng. In: *Oceanic Engineering, IEEE Journal of* 26.2 (2001), pp. 228–239. ISSN: 0364-9059.

[15] Ingrid Schjølberg. *Modeling and control of underwater robotic systems*. eng. Trondheim, 1996.

[16] Bruno Siciliano et al. *Robotics: Modelling, Planning and Control*. eng. Advanced Textbooks in Control and Signal Processing. London: Springer London, 2009. ISBN: 978-1-84628-641-4.

[17] Mark W Spong. *Robot modeling and control*. eng. Hoboken, N.J, 2006.

[18] Standard-Norge. “Remotely operated vehicle (ROV) services, norsok u-102”. In: (2003).